Aqueous Phase Photo-oxidation of Brown Carbon Nitrophenols: Reaction Kinetics, Mechanism, and Evolution of Light Absorption

Rachel F. Hems, Jonathan P. D. Abbatt

Aqueous Phase Photo-oxidation of Brown Carbon Nitrophenols: Reaction Kinetics, Mechanism, and Evolution of Light Absorption

Rachel F. Hems, Jonathan P. D. Abbatt*

Department of Chemistry, University of Toronto, 80 St. George Street, Toronto, ON, M5S 3H6, Canada

ABSTRACT

Light absorbing organic aerosol particles, referred to as brown carbon, are geographically widespread and can have an important climate impact through the absorption of solar radiation. Recent studies, both in the laboratory and the field, have shown that brown carbon aerosols can be bleached of their color by direct photolysis and photo-oxidation reactions on the timescale of hours to days. However, the photo-oxidation of nitrophenol molecules, which are colored compounds often associated with biomass burning organic aerosol, show an enhancement in light absorption before the color is lost. This study investigates the mechanism of color enhancement and the fate of three nitrophenol compounds, specifically nitrocatechol, nitroguaiacol, and dinitrophenol, in aqueous aerosol using online aerosol chemical ionization mass spectrometry (aerosol-CIMS). The second order rate constants for the three nitrophenols with OH radicals in the aqueous phase at pH

7 (298 K), were determined to be 5×10^9 $M^{-1}s^{-1}$, 5.2×10^9 $M^{-1}s^{-1}$, and 3.7×10^9 $M^{-1}s^{-1}$ for nitrocatechol, nitroguaiacol, and dinitrophenol, respectively. For a representative aqueous OH concentration, these rate constants correspond to an aqueous lifetime with respect to OH on the order of hours. While the nitrophenol molecules react rapidly with OH, the initial products, which are functionalized by additional electron-donating OH groups, likely lead to the observed absorption increase in the visible range. Further photo-oxidation fragments the aromatic structure to produce smaller, highly oxygenated molecules which no longer absorb strongly at visible wavelengths. These products include furoic acid, glyoxylic acid, malonic acid, oxalic acid, and isocyanic acid. All three nitrophenols investigated formed similar products during photo-oxidation, suggesting that these results could be generalized to this larger class of compounds.

Keywords: brown carbon aerosol, biomass burning, photo-bleaching, aqueous oxidation, aerosol aging

INTRODUCTION

Light absorbing organic aerosol particles in the atmosphere, known as brown carbon (BrC), are increasingly studied due to their various sources, complex composition, and prevalence in the atmosphere. Similar to black carbon, BrC can give rise to a positive radiative forcing through the aerosol direct effect, especially in the upper troposphere.[1] The semi-direct effect observed with black carbon, where warming can decrease relative humidity and increase cloud droplet evaporation, may also enhance the positive radiative forcing potential of BrC.[2] However, the magnitude of the warming effect of BrC is still uncertain and has only recently been investigated in models.[1,3–6] A major primary source of BrC is biomass and fossil fuel burning.[7] Secondary production can also occur through aqueous chemistry between ammonia or amines and

aldehydes,[8–10] as well as photo-oxidation of phenolic compounds.[11,12] Nitrophenols are a class of light absorbing compounds often detected in significant concentrations (10s of ng m^{-3}) in biomass burning BrC.[13,14] These phenolic compounds are derived from pyrolysis of lignin,[14] but can also be formed by photo-oxidation of anthropogenic pollutants such as xylene[15] and toluene.[16] Nitrophenols are readily water soluble and have been measured in cloud, fog, and rain water at concentrations of up to tens of ug L^{-1}.[13]

The magnitude of the climate impact of BrC depends in part on the atmospheric lifetime of the specific light-absorbing compounds. Forrister *et al*. followed a biomass burning plume downwind from the source and found a significant decrease in the BrC absorption with photochemical aging.[17] Photo-bleaching of BrC has been observed in a number of studies both in the laboratory and in field measurements.[18–22] Analysis of aged biomass burning BrC by Di Lorenzo *et al.* found no detectable nitrophenol compounds, and instead concluded that the majority of the light absorbing compounds had very large molecular weights (>1000 amu).[23,24] Nitrophenols are reactive towards direct photolysis[25–28] and photo-oxidation[29–31] in the gas phase and the condensed phase and therefore it is likely that atmospheric aging decreases their concentration. However, to account for detection of nitrophenols far from primary sources, aqueous formation of nitrophenols has also been proposed.[13]

Zhao *et al.* noted a striking feature in the aqueous OH oxidation of nitrophenol compounds during the early part of the reaction, the absorption in the visible range (and specifically at 420 nm) increased.[18] This suggests that the reaction products were just as, if not more, strongly absorbing than the parent nitrophenol molecule. This feature of enhanced absorption has also been observed more generally from atmospheric processing of biomass burning aerosol.[32,33] At longer OH oxidation times, the absorbance at all wavelengths was observed to decrease

significantly. The formation of light-absorbing products could extend the lifetime of BrC absorption even after the nitrophenol has reacted. However, this mechanism has not been previously examined.

This study investigates the photo-oxidation of three commonly detected nitrophenol compounds using the aerosol-CIMS: nitrocatechol, nitroguaiacol, and dinitrophenol (structures shown in **Figure 1**). The second-order rate constants of their reaction with OH, the change in UV-visible light absorption, and mechanistic insights are presented for all three molecules. These measurements provide a better understanding of the aging of this class of BrC compounds and how their light absorption changes as a function of that aging.

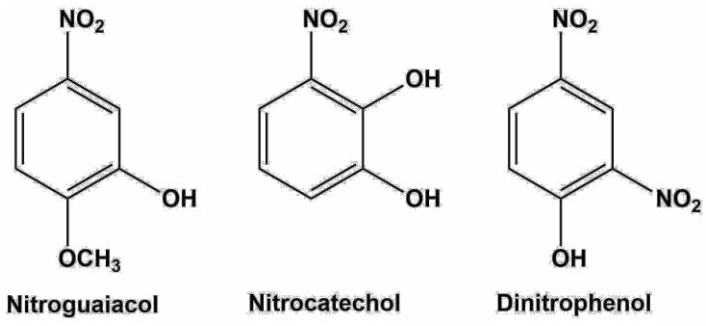

Figure 1. Chemical structures of the nitrophenols examined in this study: nitroguaiacol, nitrocatechol, and dinitrophenol.

EXPERIMENTAL METHODS

Photo-oxidation of nitrophenol compounds

Photo-oxidation reactions were carried out in a Pyrex atomizer bottle with a 254 nm mercury lamp (UVP, constructed to remove the 185 nm line to avoid generating ozone) inserted inside the reaction solution (150 mL total volume). Solutions of 4-nitrocatechol, 2-methoxy-5-nitrophenol

(5-nitroguaiacol), and 2,4-dinitrophenol (Sigma-Aldrich) were supplied from stock solutions, made with purified water (18.2 MΩ cm), to obtain a concentration of 30 μM in the reaction vessel. This concentration of nitrophenol was used to simulate the upper end of concentrations measured in biomass burning impacted cloud water.[34] H_2O_2 (≥ 30% wt, Sigma-Aldrich) as the OH precursor, was added to obtain a concentration of 1 mM. Upon UV irradiation, this concentration of H_2O_2 generated an OH radical steady state concentration of approximately $(3 – 4) \times 10^{-13}$ M in solution (see supporting information for detailed calculation). For all photo-oxidation experiments, reaction time = 0 is defined as the time that the lamp was turned on, which initiated OH radical generation. The pH of the solutions was unbuffered and was generally between 6.5 – 7.5 throughout the reaction. The pKa for 4-nitrocatechol (6.87)[35], 5-nitroguaiacol (estimated from 4-nitroguaiacol[35] ~ 7), and 2,4-dinitrophenol (4.04)[35] indicate that nitrocatechol and nitroguaiacol are likely to be present as both the ionized and non-ionized form, while dinitrophenol is expected to be primarily ionized under the experimental conditions. Any differences in the chemistry of the nitrophenol and corresponding nitrophenolate were not isolated in this study. The starting temperature of the solutions was unregulated (24±2 ºC) with some warming from the UV lamp to reach temperatures of up to 30±1 ºC, as measured by a thermometer after 60 minutes.

Aerosol-CIMS

An aerosol time-of-flight chemical ionization mass spectrometer (TOF-CIMS, Aerodyne Research Inc.) was employed for online analysis of reaction solutions during photo-oxidation. The aerosol-CIMS setup and operation has been described previously,[36–39] but will be briefly summarized here. The experimental set-up is illustrated in **Figure S1**. The reaction solution was atomized by a constant output atomizer (TSI, model 3076) using compressed air as the carrier

gas (Linde, Air Grade Zero 0.1) at a flow rate of 3 L min^{-1}. The atomizer output was diluted with a 1.5 L min^{-1} flow of nitrogen and directed through a Siltek-coated stainless steel tube (1/4 in. OD, 70 cm long, VWR) heated to 150 °C. The volatilized organic compounds were introduced into the TOF-CIMS, which had a sample flow rate of 2.0 L min^{-1} (set by a critical orifice).

The reagent ion used in this study was the acetate anion ($CH_3C(O)O^-$) due to its sensitivity towards acidic organic compounds.[40] Acetate was generated by a flow of 10 sccm of nitrogen through the headspace of acetic anhydride (Sigma-Aldrich) in a stainless steel bottle at room temperature, which was then diluted by 2.2 L min^{-1} of nitrogen. The reagent ion flow passed through a ^{210}Po radioactive cell (NRD, P-2021) at a flow of 2 L min^{-1} (set by a critical orifice) to generate acetate ions in the ion-molecule reaction (IMR) chamber of the CIMS. The acetate ion was thought to ionize primarily by proton abstraction, however, other ionization mechanisms have recently been identified.[41] The pressures in the IMR and short segmented quadrupole ion-transmission (SSQ) regions were set to 100±5 mbar and 2.0±0.1 mbar respectively. A strong-field mode is used to prevent formation of acetate clusters (detailed voltage parameters in **Table S1**), where the [acetate + acetic acid] cluster to acetate ratio is approximately 0.001. The mass spectrometer was operated in V-mode and data were acquired at 1 s time resolution. Data processing was performed in Igor Pro (WaveMetrics Inc. Version 6.37) running Tofware (Aerodyne Research Inc. Version 2.5.7). A mass accuracy of ± 5 μTh Th^{-1} (ppm) and mass resolving power of 3500 - 4500 were obtained over the relevant *m/z* range. All data are presented as the signal of the ion of interest normalized to the signal of the acetate reagent ion.

UV-Vis Analysis

Measurement of the UV-Vis absorbance of the reaction solution (2 mL aliquots) throughout the photo-oxidation experiments was performed offline on the same day as collection. A liquid waveguide capillary UV-Vis spectrometer (World Precision Instruments) was used, with a deuterium tungsten halogen light source (DT-Mini-2, Ocean Optics) and a temperature controlled UV-Vis spectrometer (USB2000+, Ocean Optics). This instrument has a long effective path length (50 cm), which results in high sensitivity. The spectrometer measures absorbance across a large spectral window, from 230 to 850 nm. SpectraSuite software (Ocean Optics) was used to record data.

Relative Rate Method

The second order rate constant of each nitrophenol compound reacting with OH radicals was determined with the relative rate method. The decay of each nitrophenol compound and the decay of a compound with a known second order rate constant with OH were measured with the aerosol-CIMS. In this study, benzoic acid (Sigma-Aldrich, 30 μM), which has a second order rate constant with OH of (5.9 ±0.5) × 10^9 M^{-1} s^{-1} at pH 7, was used as the reference compound.[42] Assuming the only loss process is reaction with OH radicals, the integrated rate law for the nitrophenol can be substituted into the integrated rate law for benzoic acid and the following relationship is obtained:

$$ln\left(\frac{[X]_0}{[X]_t}\right) = \frac{k_X^{II}}{k_{BA}^{II}} \times ln\left(\frac{[BA]_0}{[BA]_t}\right) \qquad (1)$$

In equation 1, $[X]_0$ and $[X]_t$ represents the nitrophenol signal measured at time zero and time *t* after OH reaction was initiated, respectively. The signal of benzoic acid (BA), the reference

compound, is also measured at time zero and time *t* during OH reaction. The second order rate constants for the nitrophenol compound and benzoic acid are denoted as k_X^{II} and k_{BA}^{II} respectively.

RESULTS AND DISCUSSION

UV-Vis Absorption Spectra

It has been reported that nitrocatechol and other nitrophenols undergo a change in absorbance during aqueous OH oxidation in the wavelength region between 410 – 460 nm.[18] Similarly, we have observed an enhancement in absorptivity in this region, then subsequent reduction in absorptivity during aqueous OH oxidation of nitrocatechol, nitroguaiacol, and dinitrophenol.

Figure 2(A) shows how the nitrocatechol UV-Vis absorption spectrum changes as OH oxidation time increases. For clarity, the absorption at 420 nm is plotted on the right, showing the maximum absorption occurring within the first 10 minutes of photo-oxidation time. This is plotted alongside the control reactions, including direct photolysis (purple) and dark reaction with H_2O_2 (pink), which show negligible changes to the absorbance over an equivalent timescale. The evolution of absorbance in the visible and near-visible range indicates that there is chemistry occurring which initially enhances the absorption and then degrades the chromophoric compounds resulting in a colorless solution.

The absorption evolution with photo-oxidation of nitroguaiacol and dinitrophenol are shown in **Figure 2**(B) and (C), respectively. Again, the corresponding absorbance during the control reactions for nitroguaiacol and dinitrophenol are plotted alongside on the right in **Figure 2**(B) and (C) respectively, and show negligible change over the reaction timescale. In the case of nitroguaiacol, the absorption enhancement at 420 nm is even greater than for nitrocatechol, and

the enhanced absorption extends longer into the reaction time. Dinitrophenol has a slightly different original UV-Vis absorption profile compared to nitrocatechol and nitroguaiacol, so the absorption change over time was instead monitored at 460 nm. This molecule also goes through a significant absorption enhancement during photo-oxidation before all absorption in this range is lost. Not only does the absorption change in these three molecules (and likely all nitroaromatic compounds), indicate that interesting oxidation chemistry is occurring in the atmospheric aqueous phase, it also has consequences for the longevity of this type of BrC compound, which ultimately affects the radiative forcing potential of these particles. To emphasize the effect that the increase in absorption has on the relative amount of sunlight absorbed, the product of the absorption (nitrophenol concentration of 5 μM, **Figure S2**) and estimated solar power flux as a function of wavelength was calculated and integrated from 300 – 700 nm, shown in **Figure S3** for each nitrophenol molecule as a function of photo-oxidation time. The corresponding relative increase in this value during the first few minutes of the reaction reinforces that the increase in the absorption of these molecules during photo-oxidation can significantly increase the overall absorbed sunlight.

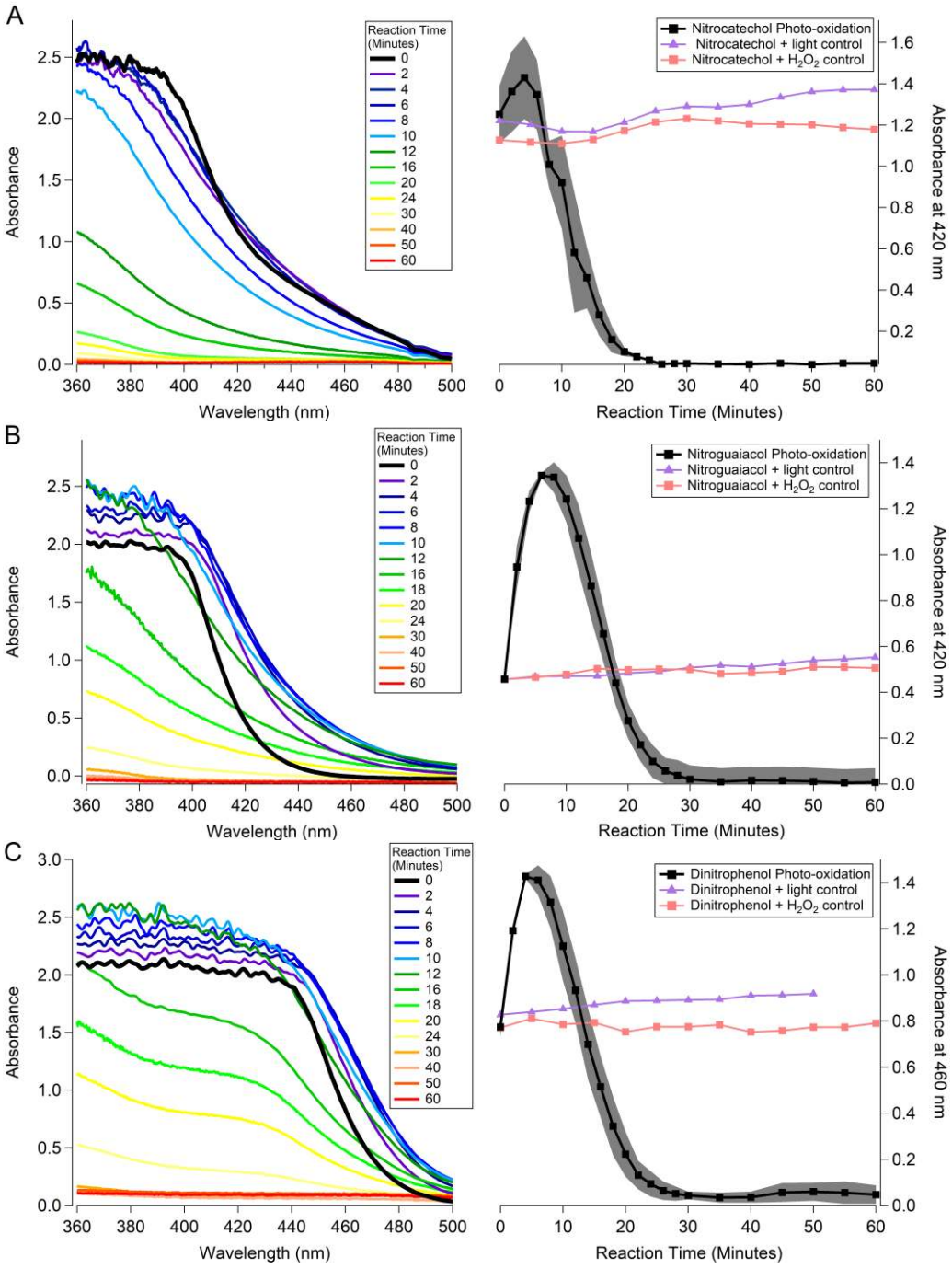

Figure 2. Absorption spectra of nitrocatechol (A), nitroguaiacol (B), and dinitrophenol (C) during photo-oxidation. On the left panel is the full spectrum taken at sequential time steps during the reaction. On the right panel, the absorbance at 420 nm (460 nm for dinitrophenol) is plotted as a function of reaction time. Shading indicates the standard deviation between multiple experiments. The control reactions including photolysis of the nitrophenol (+ light control, purple) and dark reaction with H_2O_2 (+ H_2O_2 control, pink) are plotted for reference.

Relative Rate Kinetics

As discussed above, the relative rate method was used to determine the second order rate constant for the reaction of each nitrophenol molecule with hydroxyl radicals in the aqueous phase at pH 7. All three nitrophenols decay rapidly following the initiation of hydroxyl radical production (at t = 0) (**Figure S4**). Equation 1 was used to determine the second order rate constant for each nitrophenol molecule from the slope of the relative rate plots shown in **Figure 3**.

The calculated second order rate constants are summarized in **Table 1**. The reported error includes the propagation of the uncertainty in the second order rate constant for benzoic acid (k^{II}_{BA}) and 1 standard deviation in the linear fit of the slope in the relative rate plots (**Figure 3**). The nitroguaiacol and dinitrophenol kinetics experiments were carried out with the benzoic acid reference compound in the same solution, as is generally done for relative rate kinetics. However, for nitrocatechol, interference at the same *m/z* was observed when benzoic acid was added to the same solution. The nitrocatechol rate constant was therefore calculated from experiments where nitrocatechol and benzoic acid were measured separately, but under the same conditions. This introduces additional error into the measurement of the nitrocatechol second order rate constant. This rate constant for nitrocatechol obtained from using benzoic acid as the reference was measured to be $(5.9 \pm 0.5) \times 10^9$ $M^{-1}s^{-1}$. To confirm this measurement, the nitrocatechol rate constant was also measured with levoglucosan as the reference compound, shown in **Figure S5** and discussed in the supporting information. The rate constant for nitrocatechol with levoglucosan as the reference was measured to be $(4.4 \pm 0.4) \times 10^9$ $M^{-1}s^{-1}$. To represent the variability in the nitrocatechol rate constant measurement, we propose a second order rate constant of $(5 \pm 1) \times 10^9$ $M^{-1}s^{-1}$.

The second order rate constant for the OH reaction with nitroguaiacol was measured to be (5.2 ± 0.4) × 10^9 M^{-1} s^{-1}. To the best of our knowledge, this is the first published report of an aqueous phase rate constant for reaction of OH radicals with nitrocatechol and nitroguaiacol. The rate constant for reaction of OH and dinitrophenol has been measured previously to be (2.3 ± 0.4) × 10^9 M^{-1} s^{-1} at pH 2.5[43] and (5.7 ± 0.6) × 10^9 M^{-1} s^{-1} at pH 7.[44] The rate constant determined from this experiment for dinitrophenol, (3.7 ± 0.3) × 10^9 M^{-1} s^{-1} at pH 7, is in good agreement with these previous studies.

The lifetime of each molecule, shown in **Table 1**, is calculated based on the rate constants determined here and an aqueous phase OH concentration of 1 × 10^{-14} M, which has been measured to be at the upper range of OH concentrations in cloud and fog water.[45–47] At this concentration, the lifetime in aqueous atmospheric droplets is on the order of 7.5 hours or less for all three nitrophenol molecules. When compared to the rate of gas phase OH oxidation (**Table S2)** and taking into account typical OH concentrations and liquid water content, aqueous phase OH oxidation is estimated to be the dominant sink for all three nitrophenols in cloud conditions (discussion in supporting information and **Table S3**). However, this conclusion will depend on the time spent in cloud, cloud and gas phase OH concentrations, as well as aerosol liquid water.

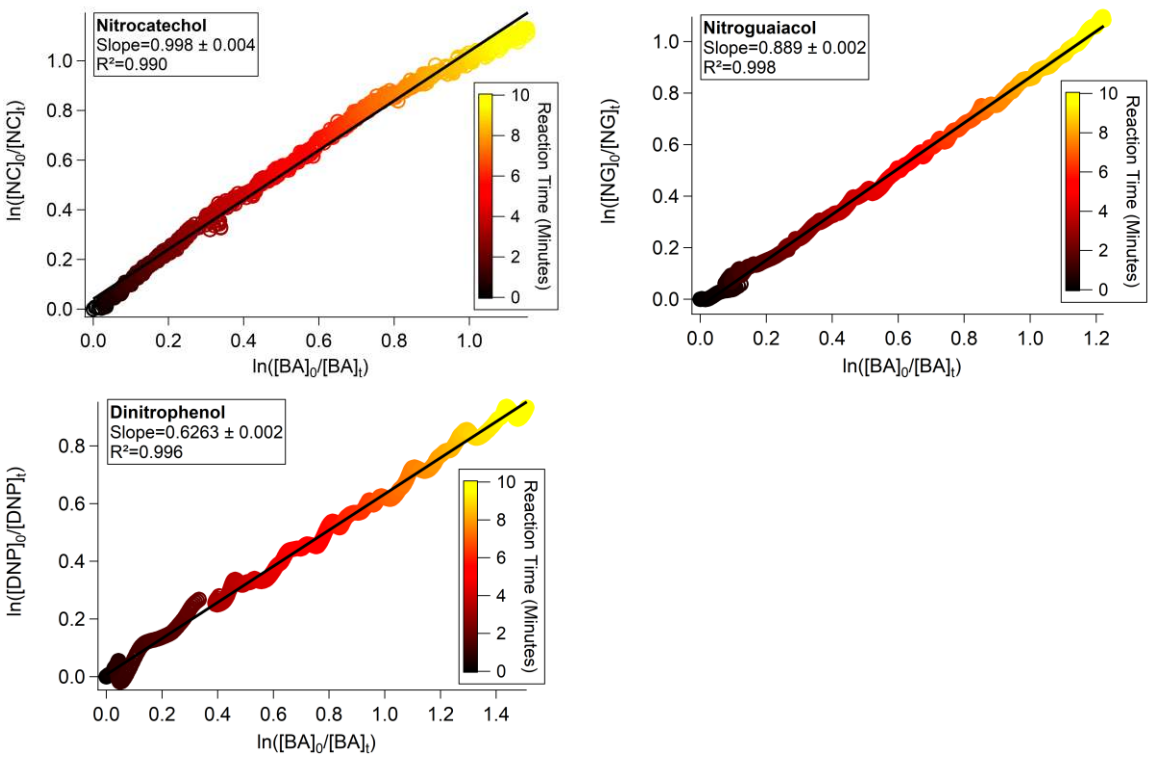

Figure 3. Relative kinetics plot of nitrocatechol, nitroguaiacol, and dinitrophenol with reference compound benzoic acid, according to Equation 1. Color scale corresponds to OH reaction time.

Table 1. Summary of nitrophenol second order rate constants and calculated aqueous phase lifetime with respect to OH oxidation at pH 7. Error on the second order rate constants is propagated from the uncertainty in the second order rate constant for benzoic acid and 1 standard deviation of the linear fits from **Figure 3**.

Molecule	**$k^{II}_{OH} \times 10^9$ ($M^{-1}s^{-1}$)** Error is based on 1 standard deviation of linear fit and uncertainty in k^{II}_{BA}	**Lifetime (hours)** Assuming [OH] = 1×10^{-14} M
4-Nitrocatechol	5 ± 1*	4.7
5-Nitroguaiacol	5.2 ± 0.4	5.3
2,4-Dinitrophenol	3.7 ± 0.3	7.5

* See discussion in Relative Rate Kinetics section regarding the uncertainty on this value.

Reaction Products and Mechanism

The formation of the photo-oxidation products of each nitrophenol molecule were monitored throughout the reaction by the aerosol-CIMS with acetate reagent ion. Approximately 50 distinct reaction products were identified by mass spectrometry as anions in each reaction (summarized in **Table S4**). No direct photolysis of the nitrophenols was observed under these conditions for the duration of the reaction (**Figure S6**). OH oxidation of chemically similar structures (benzene, phenol, and nitrophenol) has been studied previously in the aqueous phase.[48–50] Those studies report that a common first oxidation step is the addition of a hydroxyl group to the aromatic ring. Oligomers are noted to arise under high concentration conditions, such as in the aqueous phase OH oxidation of mM and higher concentration solutions of small dicarbonyls,[51,52] as well as at 100 μM concentrations of phenols.[49,53] With the nitrophenol concentrations used in this experiment (30 μM), oligomers were not observed to form.

Photo-oxidation of the more substituted nitrophenols explored in this study (nitrocatechol, nitroguaiacol, and dinitrophenol) have not been previously examined. The primary goal of elucidating the photo-oxidation mechanism is to identify possible absorbing species that may cause the observed enhancement in absorption in the visible light range (**Figure 2**). Identification of the breakdown pathway and final fate of the nitrophenol molecules is the secondary goal of elucidation of the photo-oxidation mechanism. For simplicity, the following discussion will focus on nitrocatechol. However, the mechanism for nitroguaiacol and dinitrophenol are analogous, and the formation of similar functionalized and fragmented products is included in the supporting information (**Figures S7 – S10**).

Functionalization

Nitrocatechol was detected as the negative ion at *m/z* 154 ($C_6H_4NO_4^-$). As the nitrocatechol signal decays following the initiation of OH oxidation, functionalized products with molecular formulae corresponding to increases in the number of oxygen atoms were observed to peak within the first 8 minutes of the reaction, as shown in **Figure 4** (all reported molecular formulae refer to the neutral molecule). These compounds have been identified by the number of oxygen atoms added to the parent nitrocatechol molecule (ie. +O, +2O, +3O, etc.). The formation of these products is consistent with the addition of an OH group and loss of a H atom, commonly observed with OH oxidation of an aromatic molecule.[48–50] Proposed structures for the functionalized products are shown in **Figure 5**. In **Figure 4**, the absorbance of the reaction solution at 420 nm (reproduced from **Figure 2**) is overlaid on the time series of the functionalization products to show the coincident time profiles. These profiles strongly suggest that the oxidation products containing additional hydroxyl groups are increasing or maintaining the absorption at this wavelength as nitrocatechol is being depleted. Hydroxyl groups donate electron density to an aromatic ring, which can shift the absorbance of the molecule further into the visible range of the spectrum. An example of this is shown in **Figure S11** for the molecules nitrobenzene and nitrophenol. The products corresponding to the +O to +3O are consistent with this mechanism.

It is also possible to have a structure, consistent with the observed molecular formulae for the +2O to +5O products, where the aromatic ring has opened by attack of a hydroxyl radical at an already substituted position. A proposed ring-opening mechanism is shown in **Figure S12**. This leads to a conjugated molecule with two carboxylic acid functional groups where the carbon-carbon bond is broken (see **Figure 5**). The ring-opened products, which cannot be differentiated

from the ring-closed structures of the same molecular formula, may also be forming during the photo-oxidation and must be invoked to explain the +4O and +5O products, since the ring is fully substituted after 3 functionalization steps. As these structures maintain extended conjugation, they may still contribute to the absorption at 420 nm, although their contribution is uncertain. Similar functionalized products were observed to form up to +4O and +3O for nitroguaiacol (**Figure S7**) and dinitrophenol (**Figure S9**), respectively.

Figure 6 shows the formation of a six-carbon oxidation product ($C_6H_4O_4$) with a similar time profile to the +O compounds. However, the nitro-group has been lost from this molecule. The molecular formula of this product is consistent with a dihydroxyquinone. Attack of the hydroxyl radical at the position of the nitro-group could result in the release of the NO_2 radical (which can be oxidized to nitrate) and formation of a hydroquinone, which could subsequently be oxidized to the quinone. A proposed mechanism for the loss of the nitro-group is shown in **Figure S13**. Quinones have also been observed to form from the OH oxidation of nitrobenzene.[48] The quinone absorption spectrum extends into the visible region, such that these types of products may also contribute to the observed absorption during the photo-oxidation reaction.

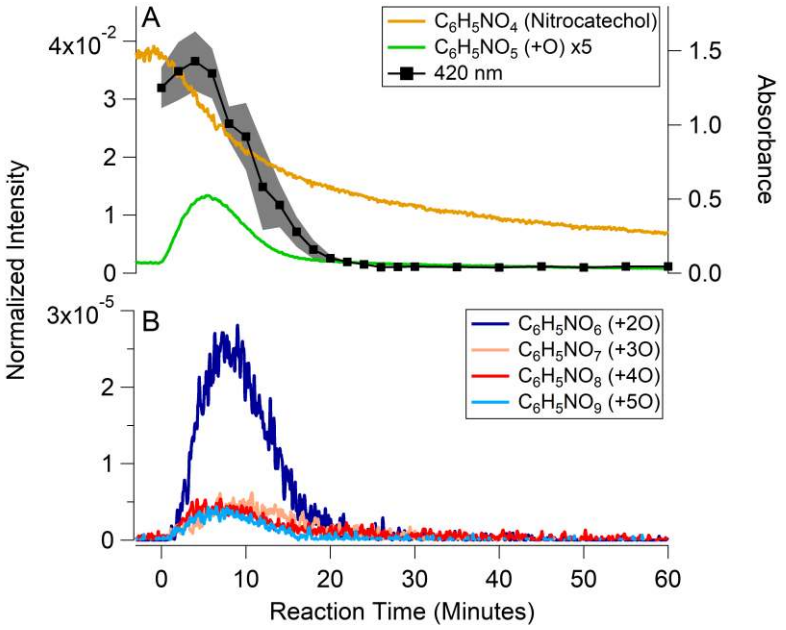

299

300 **Figure 4.** Decay of nitrocatechol and formation of functionalization products (+O products) as a
301 function of reaction time from the photo-oxidation of nitrocatechol. The signal from each
302 molecule is normalized to the acetate reagent ion and the normalized intensity is plotted for
303 nitrocatechol and the +O product in panel A (left axis), and for the +2O to +5O products in panel
304 B. The +O product intensity has been multiplied by a factor of 5, as indicated in the legend. The
305 absorption at 420 nm is reproduced from **Figure 2** and overlaid in panel A (right axis) to
306 facilitate comparison with the formation of reaction products.

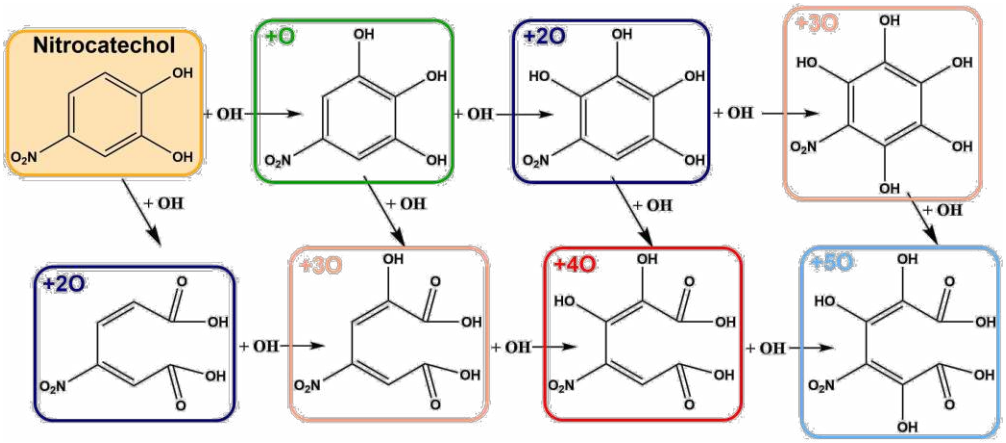

307

308 **Figure 5.** Proposed structures for the OH functionalization products of nitrocatechol photo-
309 oxidation shown in **Figure 4** (using the same color scheme). Products with +2O (dark blue) and
310 +3O (peach) have two possible structures based on the molecular formula.

Fragmentation

Figure 6 shows a selection of the observed fragmentation products from the photo-oxidation of nitrocatechol. These products correspond to carbon numbers less than that of the parent molecule (i.e., C_1 - C_5) and they have been roughly divided into time profiles which peak early (6 – 22 minutes, **Figure 6** panel A) and later (22 – 60 minutes, **Figure 6** panel B) in the reaction. Possible structures for these products are shown in **Figure 7**. Generally, molecules with carbon numbers of C_5, C_4, and C_3 formed earlier in the reaction, followed by molecules with fewer carbons (C_2, C_1). One notable exception to this is the early formation of glyoxylic acid ($C_2H_2O_3$). This indicates that as the six-carbon molecules are broken down early in the reaction, glyoxylic acid is produced along with the C_3 - C_5 compounds. Other breakdown products with and without nitrogen are observed to form early in the reaction, such as furoic acid ($C_5H_4O_3$), maleic acid ($C_4H_4O_4$), and nitroacrylic acid ($C_3H_3NO_4$) (see **Figure 6**). The identified fragmentation products are not expected to absorb strongly in the near-UV and visible range, in agreement with the observed loss of absorption at later reaction time (>10 minutes).

Many compounds that peak later in the reaction persist longer, some maintaining appreciable signal until the end of the experiment. Some of these compounds are common oxidation products such as glycolic acid ($C_2H_4O_3$), malonic acid ($C_3H_4O_4$), and oxalic acid ($C_2H_2O_4$) (see **Figure 6**). These small acids generally have slower reaction rates with OH radicals[54] and may persist in the aqueous phase. Loss of the nitro-group throughout the photo-oxidation was also observed, as indicated by the formation of nitrous acid (HNO_2) and nitric acid (HNO_3) (not shown). This has been observed previously in the OH oxidation of nitrobenzene where the nitro-group was lost from the parent molecule and phenol and benzenediols were formed.[48] In the case of nitrocatechol, benzenediols or benzenetriols were not observed to form. The peak production of

HNO_2 and HNO_3 occurs after 13 minutes and continues toward the end of the reaction time (see **Table S4**), which suggests that the nitro-group is lost after significant oxidation of nitrocatechol, from a ring-opened product or later in the reaction from a smaller fragment molecule. This mechanism is further supported by the observation of lower carbon number products which contain nitrogen in their molecular formulae, such as nitroacrylic acid ($C_3H_3NO_4$) and nitropropanoic acid ($C_3H_5NO_4$) (see **Table S4**). Similar fragmentation products to nitrocatechol were observed to form during photo-oxidation of nitroguaiacol (**Figure S8**) and dinitrophenol (**Figure S10**) with a similar pattern of larger carbon number products appearing first, followed by products with fewer carbons.

Surprisingly, isocyanic acid (HNCO) was also observed to form as a breakdown product during the photo-oxidation of nitrocatechol (**Figure 6**, panel B). Previously, HNCO has been detected as a gas phase photo-oxidation product of amines,[55,56] a class of molecules in which nitrogen is present in a reduced state (oxidation state of -3). This is the first observation of HNCO produced during aqueous phase photo-oxidation from any source, as well as the first observation of HNCO formation from a nitro-group where the nitrogen is in an oxidized state (oxidation state of +3). HNCO formation was observed from photo-oxidation of all three nitrophenol molecules, confirming that it is a common breakdown product for this class of molecules. The exact mechanism leading to the formation of HNCO remains unclear and could not be determined within the scope of this study, especially because it appears that the nitrogen atom is being photo-reduced. We cannot rule out that some signal measured as HNCO may come from ion fragmentation or thermal decomposition within the aerosol-CIMS setup. However, external calibration confirmed that dissolved HNCO could be measured directly and quantified with the aerosol-CIMS (**Figure S14**). Based on this calibration, the measured yield of HNCO from

nitrocatechol photo-oxidation at the end of the reaction was approximately 9%. There is some indication towards the end of the reaction that HNCO concentrations are decreasing, which may be due to hydrolysis. However, the observed decay cannot be fully accounted for by the hydrolysis rate (assuming a pH between 6 -7),[57] which may suggest photo-oxidation of HNCO, although the latter was not confirmed. The aqueous photo-oxidation of nitrophenols may contribute to the production of HNCO in cloud and aerosol liquid water, which can partition to the gas phase according to its Henry's law constant.[57] A photochemical source of HNCO was observed to dominate at a field site in La Jolla, California,[58] suggesting a significant unknown daytime source for HNCO. Much remains to be discovered about the aqueous sources and sinks of HNCO.

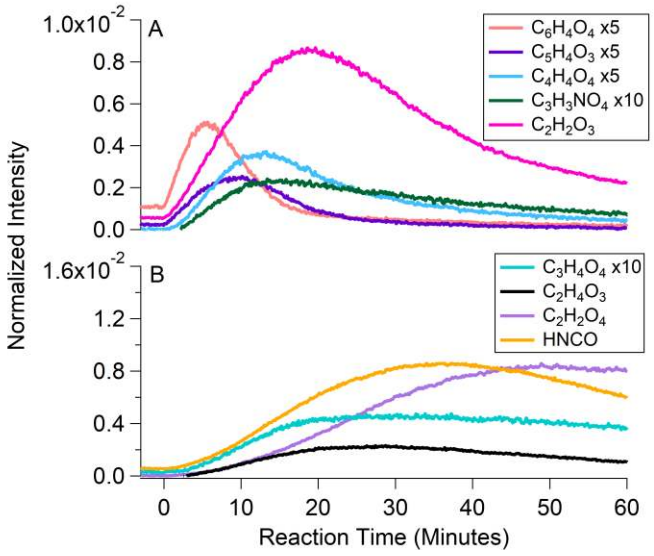

Figure 6. Formation of fragmentation products as a function of reaction time from the photo-oxidation of nitrocatechol. The signal from each molecule is normalized to the acetate reagent ion to give the normalized intensity. Panel A shows "early" fragmentation products and panel B

shows “later” fragmentation products as discussed in text. Some product intensities have been multiplied by a factor of 5 or 10 to be on scale with other molecules, as indicated in the legend.

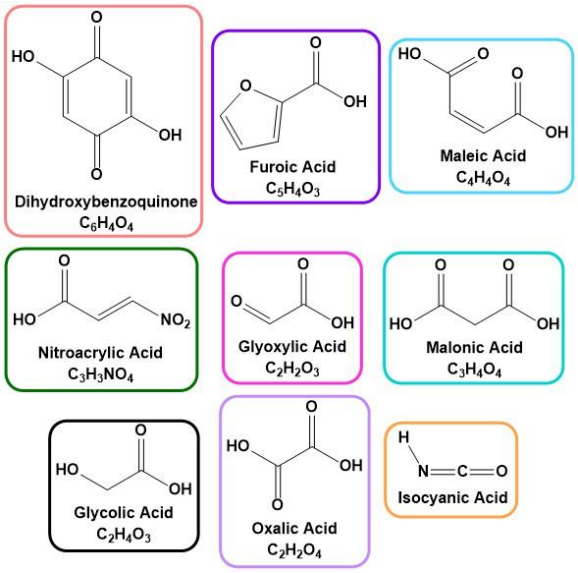

Figure 7. Proposed structures for fragmentation products formed from the photo-oxidation of nitrocatechol (time profiles shown in **Figure 6**, using the same color scheme).

CONCLUSIONS AND ENVIRONMENTAL IMPLICATIONS

Nitrophenols, specifically nitrocatechol, nitroguaiacol, and dinitrophenol, were observed to react rapidly in the aqueous phase with hydroxyl radicals. The second order rate constants were measured for each molecule and correspond to aqueous phase lifetimes on the order of hours, assuming an OH radical concentration of 1×10^{-14} M. Under cloud conditions, the rate of aqueous phase OH oxidation dominates over the rate of gas phase oxidation, making the aqueous phase an important reactive sink. This fast aqueous phase oxidation is consistent with measurements of biomass burning BrC where nitrophenols are observed close to the source, but are less concentrated or not found in aged samples further downwind of the source.[23] While we have examined aqueous phase oxidation under cloud water conditions, it is entirely likely that similar processes occur by heterogeneous oxidation.

The reaction products formed throughout the photo-oxidation of the nitrophenols were measured online with the aerosol-CIMS and the corresponding evolution of the UV-Vis absorbance spectrum was measured offline. Initially, the formation of functionalized products corresponding to the addition of OH to the parent molecule was observed. The formation of these products corresponded to the increased absorption in the visible range observed early in the reaction, even after the light-absorbing parent molecule had been significantly depleted. Later in the reaction, fragmentation products with smaller carbon numbers were observed, with signals arising from small compounds like oxalic, glycolic, and malonic acids present at sustained levels until the end of the observations. The loss of aromatic molecules through fragmentation to smaller molecules parallels the loss in absorption intensity in the visible range. Isocyanic acid (HNCO) was also observed to form during photo-oxidation of all three nitrophenols, indicating that this reaction could be a secondary photochemical source of HNCO in the aqueous phase. The majority of HNCO is thought to arise from primary emissions, although a secondary source was suggested from field observations.[58] Understanding the sources of HNCO is important because it is toxic and can react with proteins in the body through carbamylation, with a potential impact on human health.[59,60]

Although nitrophenols are observed to contribute to the light absorption in BrC aerosol from biomass burning, they are reactive towards oxidation, especially in the aqueous phase. Early steps in the reaction which functionalize the nitrophenol molecule can increase the absorption intensity, possibly increasing the atmospheric warming potential of the BrC. However, further oxidation results in the formation of smaller organic acids which no longer contribute to absorption in the visible wavelengths, thus photo-bleaching the BrC. The overall warming impact of the BrC will strongly depend on the amount of time nitrophenols spend in the

atmospheric aqueous phase and the extent of oxidation by OH radicals. Since nitrophenols are reactive towards oxidation as well as vulnerable to photolysis,[18,26,27,61] they may not contribute to long-lived BrC or significant atmospheric warming via the direct or semi-direct effects. If short-lived species, such as nitrophenols, are not present at long photochemical times then it is possible that the chemical composition of the long-lived BrC present in aged aerosol consists of less chemically reactive oligomeric species with large molecular weights.[62] We are currently extending the methods used in this paper to study the chemical reactivity of such species.

ASSOCIATED CONTENT

Supporting Information

Supporting Information Available: Additional text and figures including aerosol-CIMS set-up and voltage parameters, absorption of nitrophenols at 5 μM and calculation of the total solar power flux absorbed per solution, relative rate kinetics figures for all nitrophenols, OH concentration calculation, gas phase nitrophenol rate constants and Henry's law constants, comparison of aqueous and gaseous OH oxidation rates of nitrophenols, all identified products from photo-oxidation of nitrophenols, control experiment for direct photolysis of nitrophenols, photo-oxidation products for nitroguaiacol and dinitrophenol, UV-Visible spectrum of nitrobenzene and nitrophenol, mechanisms for OH-initiated ring opening and nitro-group loss, and aerosol-CIMS calibration for HNCO.

AUTHOR INFORMATION

Corresponding Author

*E-mail: rachel.hems@mail.utoronto.ca, Telephone: 1-416-946-7359

Author Contributions

The manuscript was written with contributions from all authors. All authors have given approval to the final version of the manuscript.

Funding Sources

This work was supported by the Natural Sciences and Engineering Research Council of Canada (NSERC).

REFERENCES

(1) Zhang, Y.; Forrister, H.; Liu, J.; Dibb, J.; Anderson, B.; Schwarz, J. P.; Perring, A. E.; Jimenez, J. L.; Campuzano-Jost, P.; Wang, Y.; et al. Top-of-Atmosphere Radiative Forcing Affected by Brown Carbon in the Upper Troposphere. *Nat. Geosci.* **2017**, *10*, 486–489.

(2) Ramanathan, V.; Carmichael, G. Global and Regional Climate Changes due to Black Carbon. *Nat. Geosci.* **2008**, *1*, 221–227.

(3) Saleh, R.; Marks, M.; Heo, J.; Adams, P. J.; Donahue, N. M.; Robinson, A. L. Contribution of Brown Carbon and Lensing to the Direct Radiative Effect of Carbonaceous Aerosols from Biomass and Biofuel Burning Emissions. *J. Geophys. Res. Atmos.* **2015**, *120* (10), 285–296.

(4) Jo, D. S.; Park, R. J.; Lee, S.; Kim, S. W.; Zhang, X. A Global Simulation of Brown Carbon: Implications for Photochemistry and Direct Radiative Effect. *Atmos. Chem. Phys.* **2016**, *16*, 3413–3432.

(5) Arola, A.; Schuster, G. L.; Pitkänen, M. R. A.; Dubovik, O.; Kokkola, H.; Lindfors, A. V.; Mielonen, T.; Raatikainen, T.; Romakkaniemi, S.; Tripathi, S. N.; et al. Direct Radiative Effect by Brown Carbon over the Indo-Gangetic Plain. *Atmos. Chem. Phys.* **2015**, *15*, 12731–12740.

(6) Feng, Y.; Ramanathan, V.; Kotamarthi, V. R. Brown Carbon: A Significant Atmospheric

Absorber of Solar Radiation. *Atmos. Chem. Phys.* **2013**, *13*, 8607–8621.

(7) Laskin, A.; Laskin, J.; Nizkorodov, S. A. Chemistry of Atmospheric Brown Carbon. *Chem. Rev.* **2015**, *115* (10), 4335–4382.

(8) Shapiro, E. L.; Szprengiel, J.; Sareen, N.; Jen, C. N.; Giordano, M. R.; McNeill, V. F. Light-Absorbing Secondary Organic Material Formed by Glyoxal in Aqueous Aerosol Mimics. *Atmos. Chem. Phys.* **2009**, *9*, 2289–2300.

(9) Lee, A. K. Y.; Zhao, R.; Li, R.; Liggio, J.; Li, S. M.; Abbatt, J. P. D. Formation of Light Absorbing Organo-Nitrogen Species from Evaporation of Droplets Containing Glyoxal and Ammonium Sulfate. *Environ. Sci. Technol.* **2013**, *47* (22), 12819–12826.

(10) Bones, D. L.; Henricksen, D. K.; Mang, S. A.; Gonsior, M.; Bateman, A. P.; Nguyen, T. B.; Cooper, W. J.; Nizkorodov, S. A. Appearance of Strong Absorbers and Fluorophores in Limonene-O_3 Secondary Organic Aerosol due to NH_4^+ -Mediated Chemical Aging over Long Time Scales. *J. Geophys. Res. Atmos.* **2010**, *115*, D05203.

(11) Chang, J. L.; Thompson, J. E. Characterization of Colored Products Formed during Irradiation of Aqueous Solutions Containing H_2O_2 and Phenolic Compounds. *Atmos. Environ.* **2010**, *44* (4), 541–551.

(12) Gelencser, A.; Hoffer, A.; Kiss, G.; Tombacz, E.; Kurdi, R.; Bencze, L. In-Situ Formation of Light-Absorbing Organic Matter in Cloud Water. *J. Atmos. Chem.* **2003**, *45* (1), 25–33.

(13) Harrison, M. A. J.; Barra, S.; Borghesi, D.; Vione, D.; Arsene, C.; Iulian Olariu, R. Nitrated Phenols in the Atmosphere: A Review. *Atmos. Environ.* **2005**, *39* (2), 231–248.

(14) Mohr, C.; Lopez-Hilfiker, F. D.; Zotter, P.; Prevot, A. S. H.; Xu, L.; Ng, N. L.; Herndon, S. C.; Williams, L. R.; Franklin, J. P.; Zahniser, M. S.; et al. Contribution of Nitrated Phenols to Wood Burning Brown Carbon Light Absorption in Detling, United Kingdom during Winter Time. *Environ. Sci. Technol.* **2013**, *47* (12), 6316–6324.

(15) Grosjean, D. Atmospheric Fate of Toxic Aromatic Compounds. *Sci. Total Environ.* **1991**, *100*, 367–414.

(16) Lin, P.; Liu, J.; Shilling, J. E.; Kathmann, S. M.; Laskin, J.; Laskin, A. Molecular Characterization of Brown Carbon (BrC) Chromophores in Secondary Organic Aerosol Generated from Photo-Oxidation of Toluene. *Phys. Chem. Chem. Phys.* **2015**, *17*, 23312–23325.

(17) Forrister, H.; Liu, J.; Scheuer, E.; Dibb, J.; Ziemba, L.; Thornhill, K. L.; Anderson, B.; Diskin, G.; Perring, A. E.; Schwarz, J. P.; et al. Evolution of Brown Carbon in Wildfire Plumes. *Geophys. Res. Lett.* **2015**, *42*, 4623–4630.

(18) Zhao, R.; Lee, A. K. Y.; Huang, L.; Li, X.; Yang, F.; Abbatt, J. P. D. Photochemical Processing of Aqueous Atmospheric Brown Carbon. *Atmos. Chem. Phys.* **2015**, *15*, 6087–6100.

(19) Lee, H. J.; Aiona, P. K.; Laskin, A.; Laskin, J.; Nizkorodov, S. A. Effect of Solar Radiation on the Optical Properties and Molecular Composition of Laboratory Proxies of Atmospheric Brown Carbon. *Environ. Sci. Technol.* **2014**, *48* (17), 10217–10226.

(20) Sareen, N.; Moussa, S. G.; McNeill, V. F. Photochemical Aging of Light-Absorbing Secondary Organic Aerosol Material. *J. Phys. Chem. A* **2013**, *117* (14), 2987–2996.

(21) Zhong, M.; Jang, M. Dynamic Light Absorption of Biomass-Burning Organic Carbon Photochemically Aged under Natural Sunlight. *Atmos. Chem. Phys.* **2014**, *14*, 1517–1525.

(22) Wong, J. P. S.; Nenes, A.; Weber, R. J. Changes in Light Absorptivity of Molecular Weight Separated Brown Carbon Due to Photolytic Aging. *Environ. Sci. Technol.* **2017**, *51* (15), 8414–8421.

(23) Di Lorenzo, R. A.; Young, C. J. Size Separation Method for Absorption Characterization in Brown Carbon: Application to an Aged Biomass Burning Sample. *Geophys. Res. Lett.* **2015**, *43*, 458–465.

(24) Di Lorenzo, R. A.; Washenfelder, R. A.; Attwood, A. R.; Guo, H.; Xu, L.; Ng, N. L.; Weber, R. J.; Baumann, K.; Edgerton, E.; Young, C. J. Molecular-Size-Separated Brown Carbon Absorption for Biomass-Burning Aerosol at Multiple Field Sites. *Environ. Sci. Technol.* **2017**, *51* (6), 3128–3137.

(25) Albinet, A.; Minero, C.; Vione, D. UVA Irradiation Induces Direct Phototransformation of 2,4-Dinitrophenol in Surface Water Samples. *Chemosphere* **2010**, *80* (7), 759–763.

(26) Zhao, S.; Ma, H.; Wang, M.; Cao, C.; Xiong, J.; Xu, Y.; Yao, S. Study on the Mechanism of Photo-Degradation of P-Nitrophenol Exposed to 254 Nm UV Light. *J. Hazard. Mater.* **2010**, *180* (1–3), 86–90.

(27) Bejan, I.; Abd-el-Aal, Y.; Barnes, I.; Benter, T.; Bohn, B.; Wiesen, P.; Kleffmann, J. The Photolysis of Ortho-Nitrophenols: A New Gas Phase Source of HONO. *Phys. Chem. Chem. Phys.* **2006**, *8* (17), 2028–2035.

(28) Chen, B.; Yang, C.; Goh, N. K. Direct Photolysis of Nitroaromatic Compounds in Aqueous Solutions. *J. Environ. Sci.* **2005**, *17* (4), 598–604.

(29) Vione, D.; Maurino, V.; Minero, C.; Duncianu, M.; Olariu, R. I.; Arsene, C.; Sarakha, M.; Mailhot, G. Assessing the Transformation Kinetics of 2- and 4-Nitrophenol in the Atmospheric Aqueous Phase. Implications for the Distribution of Both Nitroisomers in the Atmosphere. *Atmos. Environ.* **2009**, *43* (14), 2321–2327.

(30) Slade, J. H.; Knopf, D. A. Heterogeneous OH Oxidation of Biomass Burning Organic Aerosol Surrogate Compounds: Assessment of Volatilisation Products and the Role of OH Concentration on the Reactive Uptake Kinetics. *Phys. Chem. Chem. Phys.* **2013**, *15* (16), 5898–5915.

(31) Slade, J. H.; Knopf, D. A. Multiphase OH Oxidation Kinetics of Organic Aerosol : The Role of Particle Phase State and Relative Humidity. *Geophys. Res. Lett.* **2014**, *41*, 5297–5306.

(32) Sumlin, B. J.; Pandey, A.; Walker, M. J.; Pattison, R. S.; Williams, B. J.; Chakrabarty, R. K. Atmospheric Photooxidation Diminishes Light Absorption by Primary Brown Carbon Aerosol from Biomass Burning. *Environ. Sci. Technol. Lett.* **2017**, *4* (12), 540–545.

(33) Gilardoni, S.; Massoli, P.; Paglione, M.; Giulianelli, L.; Carbone, C.; Rinaldi, M.; Decesari, S.; Sandrini, S.; Costabile, F.; Gobbi, G. P.; et al. Direct Observation of Aqueous Secondary Organic Aerosol from Biomass-Burning Emissions. *Proc. Natl. Acad. Sci.* **2016**, *113* (36), 10013–10018.

(34) Desyaterik, Y.; Sun, Y.; Shen, X.; Lee, T.; Wang, X.; Wang, T.; Collett, J. L. Speciation Of "brown" carbon in Cloud Water Impacted by Agricultural Biomass Burning in Eastern

China. *J. Geophys. Res. Atmos.* **2013**, *118* (13), 7389–7399.

(35) Hinrichs, R. Z.; Buczek, P.; Trivedi, J. J. Solar Absorption by Aerosol-Bound Nitrophenols Compared to Aqueous and Gaseous Nitrophenols. *Environ. Sci. Technol.* **2016**, *50* (11), 5661–5667.

(36) Aljawhary, D.; Lee, A. K. Y.; Abbatt, J. P. D. High-Resolution Chemical Ionization Mass Spectrometry (ToF-CIMS): Application to Study SOA Composition and Processing. *Atmos. Meas. Tech.* **2013**, *6*, 3211–3224.

(37) Aljawhary, D.; Zhao, R.; Lee, A. K. Y.; Wang, C.; Abbatt, J. P. D. Kinetics, Mechanism, and Secondary Organic Aerosol Yield of Aqueous Phase Photo-Oxidation of α-Pinene Oxidation Products. *J. Phys. Chem. A* **2016**, *120* (9), 1395–1407.

(38) Zhao, R.; Mungall, E. L.; Lee, A. K. Y.; Aljawhary, D.; Abbatt, J. P. D. Aqueous-Phase Photooxidation of Levoglucosan - A Mechanistic Study Using Aerosol Time-of-Flight Chemical Ionization Mass Spectrometry (Aerosol ToF-CIMS). *Atmos. Chem. Phys.* **2014**, *14*, 9695–9705.

(39) Zhao, R.; Aljawhary, D.; Lee, A. K. Y.; Abbatt, J. P. D. Rapid Aqueous-Phase Photooxidation of Dimers in the α-Pinene Secondary Organic Aerosol. *Environ. Sci. Technol. Lett.* **2017**, *4* (6), 205–210.

(40) Veres, P.; Roberts, J. M.; Warneke, C.; Welsh-Bon, D.; Zahniser, M.; Herndon, S.; Fall, R.; de Gouw, J. Development of Negative-Ion Proton-Transfer Chemical-Ionization Mass Spectrometry (NI-PT-CIMS) for the Measurement of Gas-Phase Organic Acids in the Atmosphere. *Int. J. Mass Spectrom.* **2008**, *274* (1–3), 48–55.

(41) Brophy, P.; Farmer, D. K. Clustering, Methodology, and Mechanistic Insights into Acetate Chemical Ionization Using High-Resolution Time-of-Flight Mass Spectrometry. *Atmos. Meas. Tech.* **2016**, *9*, 3969–3986.

(42) Herrmann, H.; Schaefer, T.; Tilgner, A.; Styler, S. A.; Weller, C.; Teich, M.; Otto, T. Tropospheric Aqueous-Phase Chemistry: Kinetics, Mechanisms, and Its Coupling to a Changing Gas Phase. *Chem. Rev.* **2015**, *115* (10), 4259–4334.

(43) García Einschlag, F. S.; Carlos, L.; Capparelli, A. L. Competition Kinetics Using the UV/H_2O_2 Process: A Structure Reactivity Correlation for the Rate Constants of Hydroxyl Radicals toward Nitroaromatic Compounds. *Chemosphere* **2003**, *53* (1), 1–7.

(44) Onstein, P.; Stefan, M. I.; Bolton, J. R. Competition Kinetics Method for the Determination of Rate Constants for the Reaction of Hydroxyl Radicals with Organic Pollutants Using the UV/H_2O_2 Advanced Oxidation Technology: The Rate Constants for the Tert-Butyl Formate Ester an. *J. Adv. Oxid. Technol.* **1999**, *4* (2), 231–236.

(45) Arakaki, T.; Anastasio, C.; Kuroki, Y.; Nakajima, H.; Okada, K.; Kotani, Y.; Handa, D.; Azechi, S.; Kimura, T.; Tsuhako, A.; et al. A General Scavenging Rate Constant for Reaction of Hydroxyl Radical with Organic Carbon in Atmospheric Waters. *Environ. Sci. Technol.* **2013**, *47* (15), 8196–8203.

(46) Herrmann, H.; Hoffmann, D.; Schaefer, T.; Tilgner, A. Tropospheric Aqueous-Phase Free-Radical Chemistry: Radical Sources, Spectra, Reaction Kinetics and Prediction Tools. *ChemPhysChem* **2010**, *11* (18), 3796–3822.

(47) Ervens, B.; George, C.; Williams, J. E.; Buxton, G. V.; Salmon, G. A.; Bydder, M.;

Wilkinson, F.; Dentener, F.; Mirabel, P.; Wolke, R.; et al. CAPRAM 2.4 (MODAC Mechanism): An Extended and Condensed Tropospheric Aqueous Phase Mechanism and Its Application. *J. Geophys. Res.* **2003**, *108* (D14), 4426.

(48) Zhao, L.; Ma, J.; Sun, Z. Oxidation Products and Pathway of Ceramic Honeycomb-Catalyzed Ozonation for the Degradation of Nitrobenzene in Aqueous Solution. *Appl. Catal. B Environ.* **2008**, *79* (3), 244–253.

(49) Sun, Y. L.; Zhang, Q.; Anastasio, C.; Sun, J. Insights into Secondary Organic Aerosol Formed via Aqueous-Phase Reactions of Phenolic Compounds Based on High Resolution Mass Spectrometry. *Atmos. Chem. Phys.* **2010**, *10*, 4809–4822.

(50) Bing, C.; Chun, Y.; Khang, G. O. H. N. Photolysis Pathway of Nitroaromatic Compounds in Aqueous Solutions in the UV/H_2O_2 Process. *J. Environ. Sci.* **2006**, *18* (6), 1061–1064.

(51) Carlton, A. G.; Turpin, B. J.; Altieri, K. E.; Seitzinger, S.; Reff, A.; Lim, H. J.; Ervens, B. Atmospheric Oxalic Acid and SOA Production from Glyoxal: Results of Aqueous Photooxidation Experiments. *Atmos. Environ.* **2007**, *41* (35), 7588–7602.

(52) Tan, Y.; Perri, M. J.; Seitzinger, S. P.; Turpin, B. J. Effects of Precursor Concentration and Acidic Sulfate in Aqueous Glyoxal - OH Radical Oxidation and Implications for Secondary Organic Aerosol. *Environ. Sci. Technol.* **2009**, *43* (21), 8105–8112.

(53) Yu, L.; Smith, J.; Laskin, A.; Anastasio, C.; Laskin, J.; Zhang, Q. Chemical Characterization of SOA Formed from Aqueous-Phase Reactions of Phenols with the Triplet Excited State of Carbonyl and Hydroxyl Radical. *Atmos. Chem. Phys.* **2014**, *14* (24), 13801–13816.

(54) Herrmann, H. Kinetics of Aqueous Phase Reactions Relevant for Atmospheric Chemistry. *Chem. Rev.* **2003**, *103* (12), 4691–4716.

(55) Borduas, N.; Abbatt, J. P. D.; Murphy, J. G. Gas Phase Oxidation of Monoethanolamine (MEA) with OH Radical and Ozone: Kinetics, Products, and Particles. *Environ. Sci. Technol.* **2013**, *47* (12), 6377–6383.

(56) Borduas, N.; Da Silva, G.; Murphy, J. G.; Abbatt, J. P. D. Experimental and Theoretical Understanding of the Gas Phase Oxidation of Atmospheric Amides with OH Radicals: Kinetics, Products, and Mechanisms. *J. Phys. Chem. A* **2015**, *119* (19), 4298–4308.

(57) Borduas, N.; Place, B.; Wentworth, G. R.; Abbatt, J. P. D.; Murphy, J. G. Solubility and Reactivity of HNCO in Water: Insights into HNCO's Fate in the Atmosphere. *Atmos. Chem. Phys.* **2016**, *16*, 703–714.

(58) Zhao, R.; Lee, A. K. Y.; Wentzell, J. J. B.; McDonald, A. M.; Toom-Sauntry, D.; Leaitch, W. R.; Modini, R. L.; Corrigan, A. L.; Russell, L. M.; Noone, K. J.; et al. Cloud Partitioning of Isocyanic Acid (HNCO) and Evidence of Secondary Source of HNCO in Ambient Air. *Geophys. Res. Lett.* **2014**, *41* (19), 6962–6969.

(59) Wang, Z.; Nicholls, S. J.; Rodriguez, E. R.; Kummu, O.; Hörkkö, S.; Barnard, J.; Reynolds, W. F.; Topol, E. J.; DiDonato, J. A.; Hazen, S. L. Protein Carbamylation Links Inflammation, Smoking, Uremia and Atherogenesis. *Nat. Med.* **2007**, *13* (10), 1176–1184.

(60) Roberts, J. M.; Veres, P. R.; Cochran, A. K.; Warneke, C.; Burling, I. R.; Yokelson, R. J.; Lerner, B.; Gilman, J. B.; Kuster, W. C.; Fall, R.; et al. Isocyanic Acid in the Atmosphere and Its Possible Link to Smoke-Related Health Effects. *Proc. Natl. Acad. Sci.* **2011**, *108*

(22), 8966–8971.

(61) Barsotti, F.; Bartels-Rausch, T.; De Laurentiis, E.; Ammann, M.; Brigante, M.; Mailhot, G.; Maurino, V.; Minero, C.; Vione, D. Photochemical Formation of Nitrite and Nitrous Acid (HONO) upon Irradiation of Nitrophenols in Aqueous Solution and in Viscous Secondary Organic Aerosol Proxy. *Environ. Sci. Technol.* **2017**, *51* (13), 7486–7495.

(62) Saleh, R.; Robinson, E. S.; Tkacik, D. S.; Ahern, A. T.; Liu, S.; Aiken, A. C.; Sullivan, R. C.; Presto, A. A.; Dubey, M. K.; Yokelson, R. J.; et al. Brownness of Organics in Aerosols from Biomass Burning Linked to Their Black Carbon Content. *Nat. Geosci.* **2014**, *7*, 647–650.

Table of Contents Graphic:

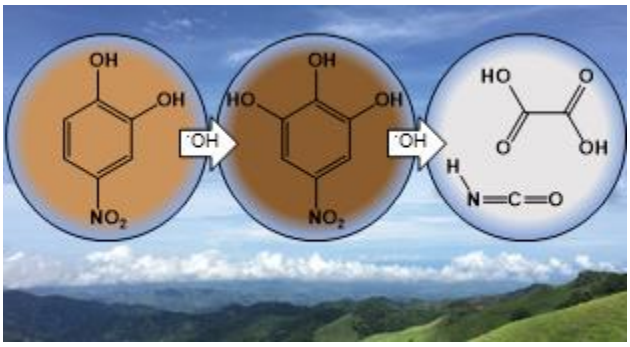

Supporting Information for:

Aqueous Phase Photo-oxidation of Brown Carbon Nitrophenols: Reaction Kinetics, Mechanism, and Evolution of Light Absorption

Rachel F. Hems[1]*, Jonathan P. D. Abbatt[1]

* Corresponding Author: Email: rachel.hems@mail.utoronto.ca, Telephone: 1-416-946-7359

[1]Department of Chemistry, University of Toronto, 80 St. George Street, Toronto, ON, M5S 3H6, Canada

Calculation of OH radical steady state concentration

The steady state OH concentration ($[OH]_{ss}$) was calculated based on the pseudo-first order decay of benzoic acid (BA), which has a known second order rate constant with OH. The equation for the pseudo-first order decay (1), the relationship between the pseudo-first order rate constant and the second order rate constant (2), and the integrated first order decay (3) are shown below:

$$-\frac{d[BA]}{dt} = k^{I}[BA] \qquad (1)$$

$$k^{I} = k^{II}[OH]_{ss} \qquad (2)$$

$$ln\left(\frac{[BA]_t}{[BA]_0}\right) = -k^{I}t \qquad (3)$$

A plot of the left side of equation 3 as a function of time gives the pseudo-first order rate constant (k^{I}). Using equation 2, and the second order rate constant for benzoic acid ($5.9 \pm 0.5 \times 10^9$ $M^{-1}s^{-1}$)[1] the concentration of OH can be calculated. The OH steady state concentration was determined to be $(3 - 4) \times 10^{-13}$ M.

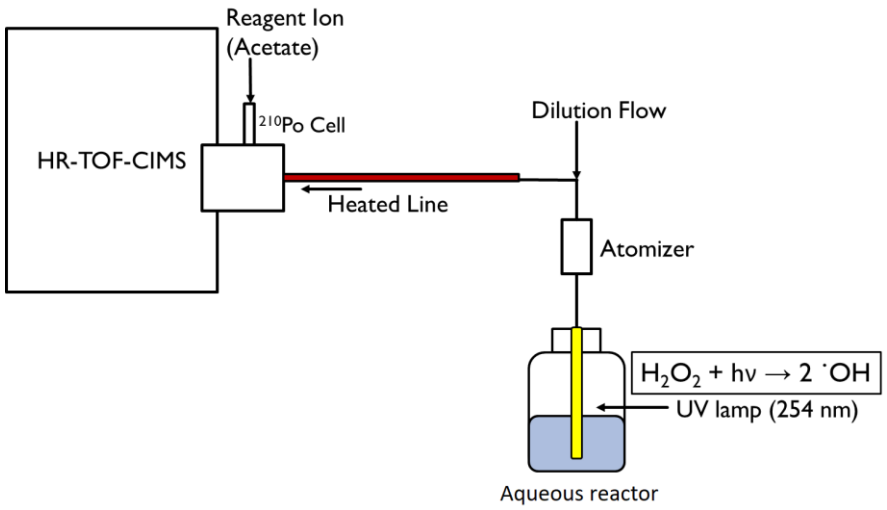

Figure S1. Experimental set-up of the aerosol-CIMS for online analysis of aqueous phase oxidation of nitrophenol molecules.

Table S1. CIMS voltage and RF parameters for strong-field mode.

Component	**Setting**	**Component**	**Setting**
IMR	0 V	RF Ampl. 1	0.24
Nozzle	3.333 V	RF 1	3090000 Hz
Q1 Entr. Pl	6.634 V	RF Ampl. 2	3.0
Q1 Front	17.935 V	RF 2	4300000 Hz
Q1 Back	-8.056 V	U+ low	700 V
Lens Skimmer	-7.233 V	U+ high	35 V
Skimmer	-1.38 V	U- low	50 V
Q2 Front	8.28 V	U- high	680 V
Q2 Back	7.164 V	Lens	1500 V
Skimmer 2	11.403 V	Drift	3000 V
Reference	48.383 V	Refl. Grid	657 V
Ion Lens	97.89 V	Refl. Backplane	700 V
Defl. Flange	38.85 V	Hardmirror	0 V
Deflector	41.504 V	Post Acc.	2700 V

Absorption of nitrophenols at a lower concentration (5 μM) and calculation of the product of nitrophenol absorption and solar power flux

The evolution of absorption for nitrocatechol, nitroguaiacol, and dinitrophenol was measured at a lower concentration (5 μM) than presented in the manuscript (30 μM) to allow for accurate measurement across the entire wavelength range. The measurement at 30 μM optimized the sensitivity of the absorption in the 400 - 500 nm range, however the absorbance below 400 nm was saturated and could not be accurately measured. The change in the absorbance spectra as a function of reaction time is shown in **Figure S2** for the three nitrophenols.

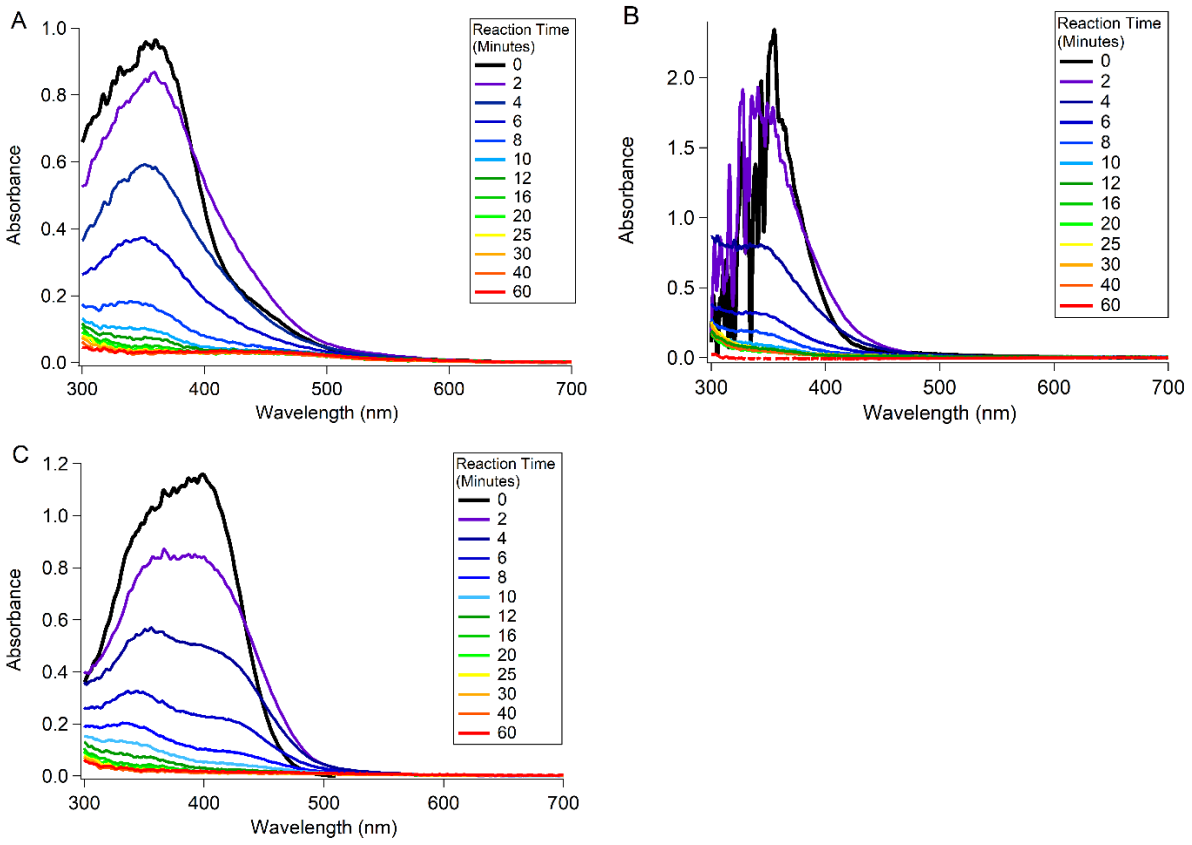

Figure S2. Absorption spectra of nitrocatechol (A), nitroguaiacol (B), and dinitrophenol (C) during photo-oxidation at a reduced concentration of 5 µM.

To examine the relative effect of the absorption change in the nitrophenols during the photo-oxidation reaction on the amount of sunlight absorbed, the product of the specific nitrophenol absorption in solution and typical solar power flux has been calculated and integrated across wavelengths between 300 – 700 nm according to the following equation:

$$Total\ solar\ power\ flux\ absorbed\ per\ solution = \int_{300\ nm}^{700\ nm} SolarPowerFlux(\lambda) \times Absorbance(\lambda)\, d\lambda \quad (4)$$

The solar power flux (irradiance, units of W m^{-2} nm^{-1}) was calculated as the total downwelling radiation using the National Center for Atmospheric Research's "Quick TUV Calculator", available here: http://cprm.acom.ucar.edu/Models/TUV/Interactive_TUV/. The following parameters were used: SZA = 0º, overhead ozone column = 300 Dobson units, surface albedo = 0.1, and ground elevation = 0 km.

The product of the solar power flux and the absorbance for each nitrophenol molecule is presented as a function of reaction time in **Figure S3**. The trend of increased intensity in the first few minutes of the reaction is carried through in this parameter for nitrocatechol and nitroguaiacol, indicating that the increased absorbance between 400 – 500 nm that the nitrophenols exhibit during photo-oxidation can cause a significant increase in the relative amount of sunlight absorbed by these compounds across the spectrum. While for dinitrophenol, the increased absorbance between 400 -500 nm during photo-oxidation slows the decline in the relative amount of sunlight absorbed.

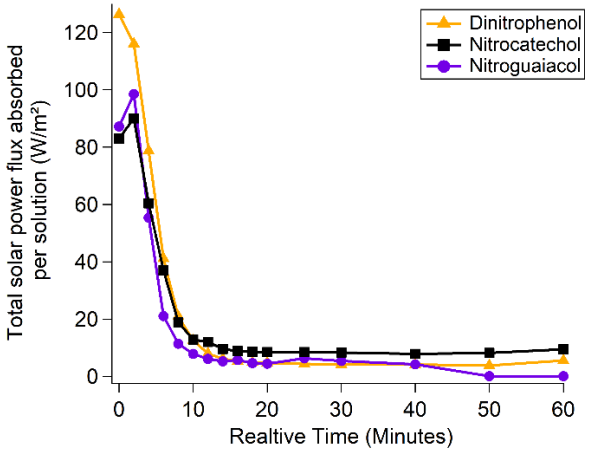

Figure S3. The product of molecular absorption and solar flux, integrated across wavelengths 300 – 700 nm as a function of OH reaction time for nitrocatechol, nitroguaiacol, and dinitrophenol.

Relative Rate Kinetics – Kinetic decay plots of nitrocatechol, nitroguaiacol, and dinitrophenol with benzoic acid as the reference compound

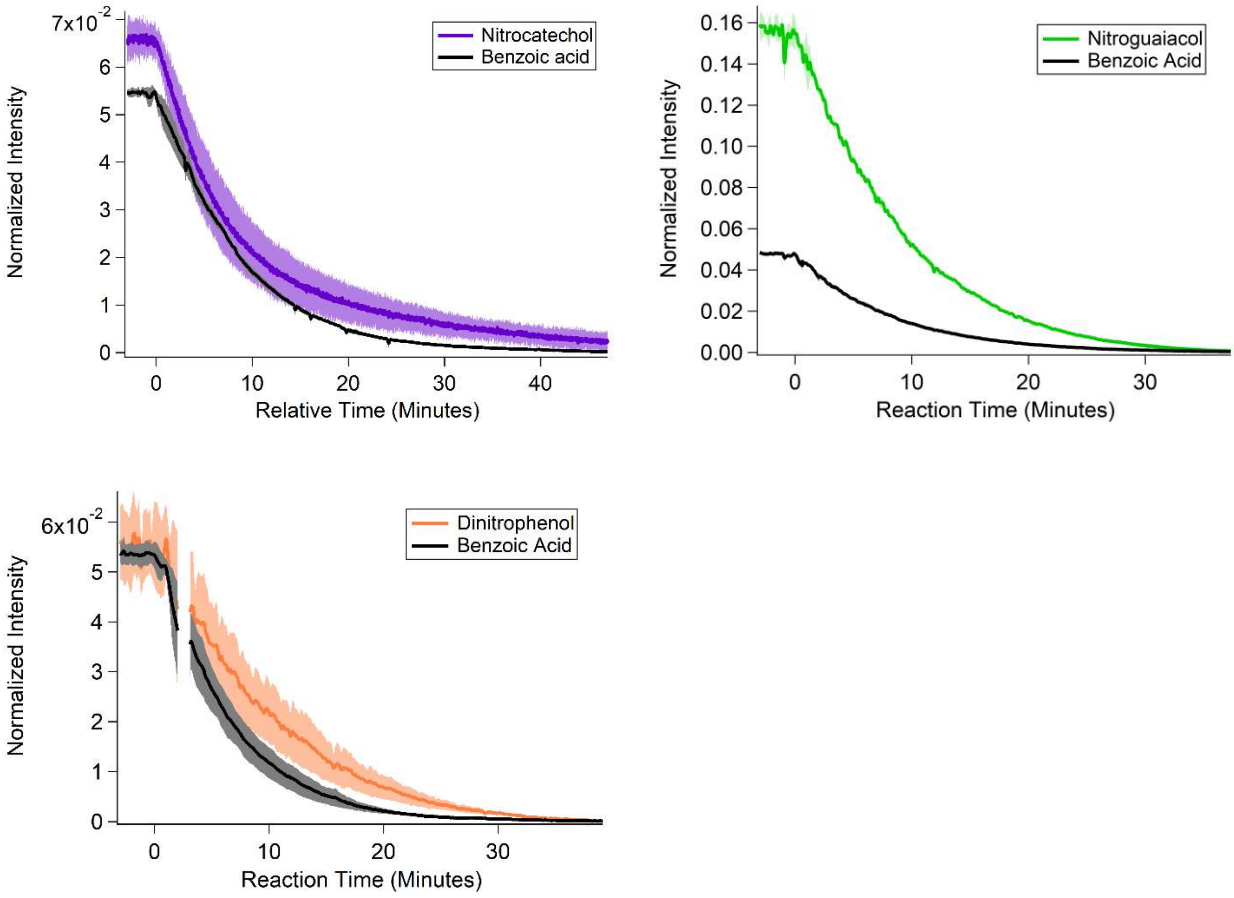

Figure S4. Nitrocatechol, nitroguaiacol, and dinitrophenol relative decay with OH reaction time, with benzoic acid as the reference compound. The average of multiple (≥2) experiments is presented with one standard deviation shown as the shading.

Relative Rate Kinetics – Nitrocatechol with levoglucosan as the reference compound

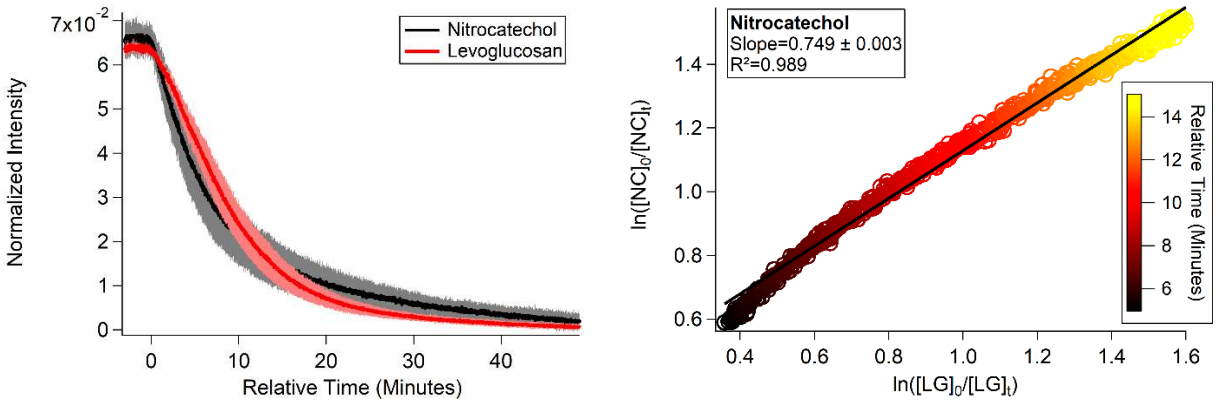

Figure S5. Nitrocatechol relative rate decay with levoglucosan as the reference compound (left). The average of multiple (≥2) experiments is presented with one standard deviation shown as the shading. Relative rate kinetics plot of nitrocatechol and levoglucosan (right). Colour scale corresponds to OH reaction time.

Levoglucosan was used as a reference compound for the measurement of the nitrocatechol second order rate constant to confirm the measurements with benzoic acid as the reference compound. The voltages in the CIMS were adjusted to favour complexation of the acetate reagent ion with the analytes. Levoglucosan was detected as its cluster with acetate (*m/z* 221), while nitrocatechol was still detected as the negative ion (*m/z* 154). Due to the lower volatility of levoglucosan, the decay was observed to be delayed, likely from desorption of levoglucosan from the heated line in the aerosol-CIMS setup. This phenomenon of delayed levoglucosan decay was observed previously with the same set-up in our laboratory.[2] Due to this delay, the relative rate was calculated for data from a relative time of 5-15 minutes, resulting in a relative rate kinetics plot (**Figure S5**, right) that does not extend to 0,0 on the x- and y-axes. The deviation from perfect 1st order decay can explain the non-linearity in the relative rate kinetics plot and introduces additional uncertainty to the measurement.

The second order rate constant for nitrocatechol with OH radical, using levoglucosan as the reference compound was calculated to be: $k^{II}_{OH} = (4.4 \pm 0.4) \times 10^9\ M^{-1}s^{-1}$. This value is similar to the value for nitrocatechol measured with benzoic acid as the reference compound, although it is not within the experimental error. Due to the challenges associated with this measurement, we

suggest the rate constant should have a larger reported error to include the variability between the two reference compounds. The second order rate constant for nitrocatechol with OH radical we report is 5 (± 1) × 10^9 $M^{-1}s^{-1}$, as discussed in the manuscript relative rate kinetics section.

Comparison of the aqueous and gaseous OH oxidation rates of nitrophenols under cloudy conditions

To compare the relative importance of the OH oxidation of nitrocatechol, nitroguaiacol, and dinitrophenol in the aqueous and gas phase, the ratio (W) of the rate of gas phase OH oxidation and the rate of aqueous phase OH oxidation was calculated according to the analysis in Epstein and Nizkorodov[3], and shown in the equation below:

$$W = \frac{\frac{dn_X^{gas}}{dt}}{\frac{dn_X^{aq}}{dt}} = (LWC_V \times K_H \times R \times T)^{-1} \times \left(\frac{k_{X+OH}^{gas}}{k_{X+OH}^{aq}}\right) \times \left(\frac{C_{OH}^{gas}}{C_{OH}^{aq}}\right) \quad (5)$$

Where LWC_V is the volume based liquid water content, in units of volume of water per volume of air. A representative value of LWC = 0.5 g m^{-3} ($LWC_V = 5\times10^{-4}$ L m^{-3}) was used based on previous measurements and the analysis in Epstein and Nizkorodov.[3] K_H is the Henry's law constant for the nitrophenol species in units of mol atm^{-1} L^{-1} (**Table S2**), R is the gas constant in units of m^3 atm K^{-1} mol^{-1}, and T is temperature, which was set to 298 K. k_{X+OH}^{gas} is the gas phase rate constant for the reaction of the nitrophenol with OH (as predicted by EPISuite, listed in **Table S2**), k_{X+OH}^{aq} is the aqueous phase rate constant for the reaction of the nitrophenol with OH, as measured in this study. C_{OH}^{gas} is the gas phase OH concentration, which was set to be a value of 1×10^6 molec cm^{-3}, and C_{OH}^{aq} is the aqueous phase OH concentration, which was set to a value of 1×10^{-14} M.

The calculated ratios (W) for each nitrophenol molecule are listed in **Table S3**. For all the nitrophenol molecules, W is less than 1, indicating that the aqueous phase OH oxidation is dominant over gas phase OH oxidation. These ratios seem to be largely driven by the Henry's law constants for these molecules which indicate that they largely favor the aqueous phase. This simple analysis does not take into account the variability in the LWC, or the aqueous and gas phase concentrations of OH. The sink by OH oxidation of the nitrophenols will depend on the amount of liquid water, the OH concentrations, as well as the temporal variability of these two factors. This

calculation does not consider any direct photolysis, which may also be a nitrophenol sink in the gas and aqueous phases.

Table S2. Gas phase second order rate constants of nitrophenol compounds with OH radicals and Henry's law constants, predicted from EPISuite, and calculated gas phase lifetime.

Molecule	**k^{II}_{OH} (cm^3 $molec^{-1}$ sec^{-1})**	**Lifetime (hours)** Assuming [OH] = $1x10^6$ molec/cm^3	**Henry's law constant, K_H (mol atm^{-1} L^{-1})**
4-Nitrocatechol	3.15×10^{-12}	88.2	4.69×10^{5}
5-Nitroguaiacol	3.49×10^{-12}	79.6	2.25×10^{5}
2,4-Dinitrophenol	0.66×10^{-12}	420.9	1.16×10^{4}

Table S3. Ratio (W) of the rate of gas phase OH oxidation and the rate of aqueous phase OH oxidation for nitrocatechol, nitroguaiacol, and dinitrophenol, as calculated from equation 5.

Molecule	**W (unitless)**
4-Nitrocatechol	1.10×10^{-2}
5-Nitroguaiacol	2.44×10^{-2}
2,4-Dinitrophenol	1.25×10^{-1}

Table S4. Identified products from photo-oxidation of nitrophenols.

m/z	**Molecular Formula (anion)**	**Proposed Identity**	**Peak Time (Minutes)**		
			Nitrocatechol	**Nitroguaiacol**	**Dinitrophenol**
42	NCO	Isocyanic acid	36.0	54.4	45.0
45	CHO_2	Formic acid	N/A	19.8	20.3
46	NO_2	Nitrous acid	13.7	25.1	18.8
61	CHO_3	Carbonic acid	47.9	76.3 (end)	50.2 (end)

62	NO_3	Nitric acid	66.7 (end)	76.3 (end)	50.2 (end)
68	C_3H_2NO	Possible: Isocyanatoethene, Isoxazole	7.2	9.7	11.6
73	C_2HO_3	Glyoxylic acid	18.5	29.4	23.8
75	$C_2H_3O_3$	Glycolic acid	26.0	49.7	28.9
84	$C_3H_2NO_2$	Possible: Acetyl isocyanate, Isoxazolone, Cyanoacetic acid	11.8	17.0	16.2
88	$C_2H_2NO_3$	Nitroethenol	66.7 (end)	76.3 (end)	27.5
89	C_2HO_4	Oxalic acid	48.4	76.3 (end)	50.2 (end)
93	C_6H_5O	Phenol	N/A	N/A	N/A
96	$C_4H_2NO_2$	Possible: Nitrosofuran, Cyanoacrylic acid	7.4	11.2	10.7
102	$C_3H_4NO_3$	Possible: Nitroacetone, Nitropropanal	9.1	18.1	13.9
103	$C_3H_3O_4$	Malonic acid	25.6	34.6	22.5
109	$C_6H_5O_2$	Catechol	N/A	N/A	N/A
111	$C_5H_3O_3$	Furoic acid	9.5	17.0	12.7
112	$C_4H_2NO_3$	Nitrofuran	7.0	11.9	13.2
114	$C_4H_4NO_3$	Possible: Nitrobutenone, Nitrodihydrofuran	8.9	15.7	15.9
115	$C_4H_3O_4$	Maleic acid	12.0	22.2	17.2
116	$C_3H_2NO_4$	Possible: Nitroacrylic acid, Nitromalonaldehyde	13.8	23.8	19.0
116	$C_4H_6NO_3$	Possible: Nitrobutanone	N/A	27.7	N/A
118	$C_3H_4NO_4$	Nitropropanoic acid	14.3	23.2	N/A
123	$C_6H_3O_3$	Hydroxybenzoquinone	N/A	4.9	5.3
123	$C_7H_7O_2$	Guaiacol	N/A	N/A	N/A

124	$C_6H_4O_3$	Trihydroxybenzene	N/A	6.6	6.2
127	$C_5H_3O_4$	Possible: Dioxopentenoic acid, Hydroxyfuroic acid	11.0	17.9	14.7
130	$C_4H_4NO_4$	Possible: Methyl-nitroacrylic acid, Hydroxyimino-oxobutanoic acid	7.4	20.1	15.7
134	$C_3H_4NO_5$	Hydroxynitropropanoic acid	25.3	N/A	N/A
138	$C_6H_4NO_3$	Nitrophenol	N/A	N/A	N/A
139	$C_6H_3O_4$	Dihydroxy-benzoquinone	5.3	8.0	9.5
139	$C_7H_7O_3$	Methoxy-benzenediol	N/A	N/A	N/A
140	$C_5H_2NO_4$	Nitrofurfual	6.6	9.8	10.1
141	C_5HO_5	Possible: Croconic acid	16.8	22.7	19.8
141	$C_6H_5O_4$	Possible: Tetrahydroxybenzene, Muconic acid	13.5	N/A	18.3
154	$C_6H_4NO_4$	Nitrocatechol	0	N/A	6.0
156	$C_7H_8O_4$	?	N/A	8.5	N/A
158	$C_5H_4NO_5$	Possible: Hydroxy-nitro-pentadienoic acid	N/A	23.2	10.7
168	$C_6H_2NO_5$	?	N/A	N/A	7.0
168	$C_7H_6NO_4$	Nitroguaiacol	N/A	0.0	N/A
169	$C_6H_3NO_5$	?	4.4	N/A	7.4
170	$C_6H_4NO_5$	Nitrocatechol + O	5.4	N/A	8.7
172	$C_6H_6NO_5$	Possible: Hydroxy-nitromethyl-pyranone, Methoxycarbonyl-dihydro-oxazole carboxylic acid	16.8	7.0	N/A
176	$C_8H_4N_2O_3$	?	N/A	21.4	N/A

181	$C_3H_5N_2O_7$	Possible: Dinitroglycerin	N/A	11.6	6.3
181	$C_9H_9O_4$	Possible: Dihydroxybenzenepropionic acid	4.6	N/A	N/A
183	$C_6H_3N_2O_5$	Dinitrophenol	N/A	5.3	0.0
184	$C_7H_6NO_5$	Nitroguaiacol + O	N/A	6.9	N/A
185	$C_{10}H_5N_2O_2$	?	N/A	7.2	N/A
186	$C_6H_4NO_6$	Nitrocatechol + 2O	8.2	N/A	N/A
199	$C_6H_3N_2O_6$	Dinitrophenol + O	N/A	N/A	6.8
200	$C_7H_6NO_6$	Nitroguaiacol + 2O	N/A	10.3	N/A
202	$C_6H_4NO_7$	Nitrocatechol + 3O	8.2	N/A	N/A
215	$C_6H_3N_2O_7$	Dinitrophenol + 2O	N/A	N/A	9.9
216	$C_7H_6NO_7$	Nitroguaiacol + 3O	N/A	15.0	N/A
218	$C_6H_4NO_8$	Nitrocatechol + 4O	5.3	N/A	N/A
231	$C_6H_3N_2O_8$	Dinitrophenol + 3O	N/A	N/A	11.3
232	$C_7H_6NO_8$	Nitroguaiacol + 4O	N/A	14.7	N/A
234	$C_6H_4NO_9$	Nitrocatechol + 5O	6.6	N/A	N/A
247	$C_6H_3N_2O_9$	Dinitrophenol + 4O	N/A	N/A	N/A
248	$C_7H_6NO_9$	Nitroguaiacol + 5O	N/A	N/A	N/A
263	$C_6H_3N_2O_{10}$	Dinitrophenol + 5O	N/A	N/A	N/A

149

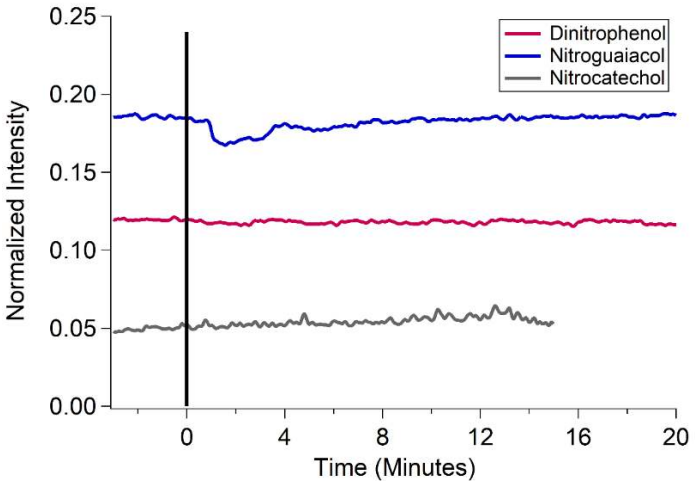

Figure S6. Nitrophenol signals as a function of time exposed to the UV lamp (254 nm) used in photo-oxidation experiments. At time = 0 minutes, the lamp was turned on. Direct photolysis was not observed under these conditions.

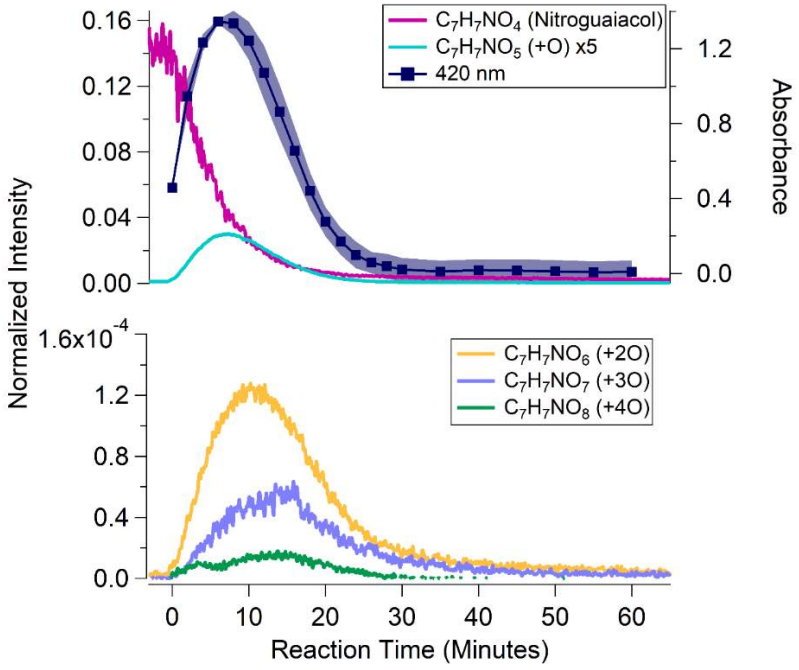

Figure S7. Decay of nitroguaiacol and formation of functionalization products (+O products) as a function of reaction time from photo-oxidation of nitroguaiacol. The signal from each molecule is normalized to the acetate reagent ion to give the normalized intensity (left axes). The absorption at 420 nm is reproduced from **Figure 2** and overlaid in the top panel (right axis) for comparison to reaction products.

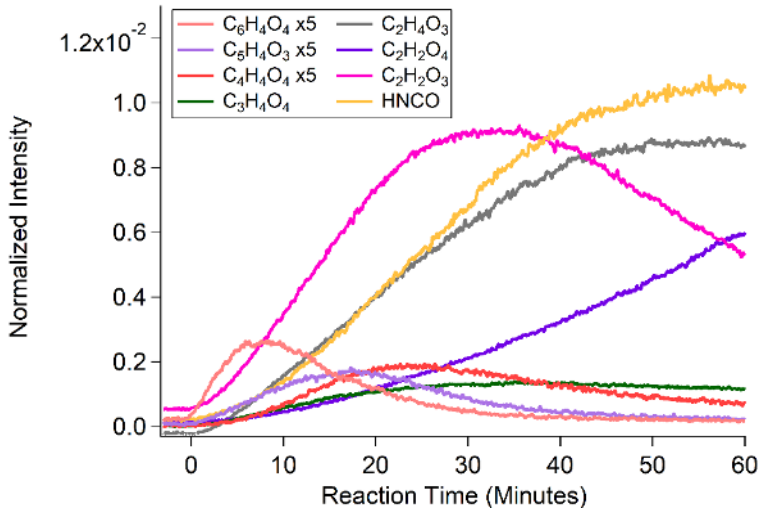

160

161 **Figure S8.** Formation of fragmentation products as a function of reaction time from the photo-
162 oxidation of nitroguaiacol. The signal from each molecule is normalized to the acetate reagent ion
163 to give the normalized intensity.

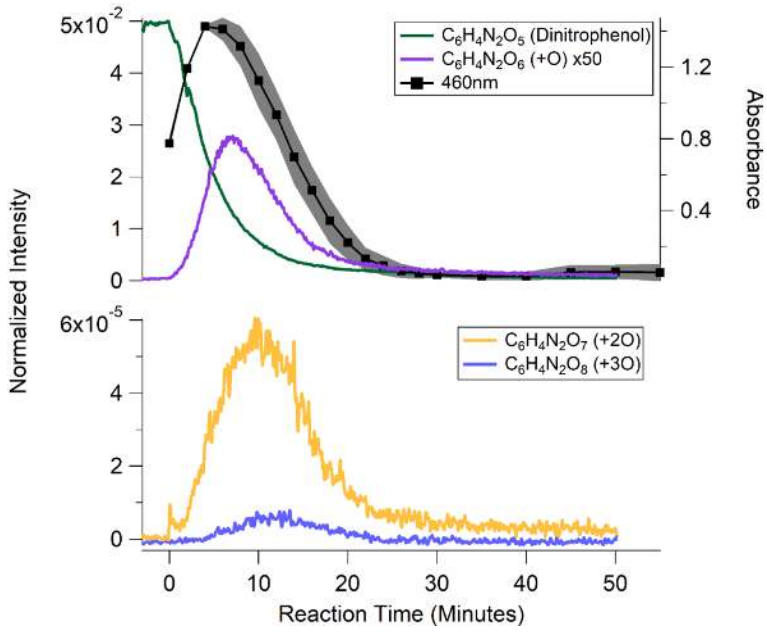

164

165 **Figure S9.** Decay of dinitrophenol and formation of functionalization products (+O products) as
166 a function of reaction time from photo-oxidation of dinitrophenol. The signal from each molecule
167 is normalized to the acetate reagent ion to give the normalized intensity (left axes). The absorption
168 at 460 nm is reproduced from **Figure 2** and overlaid in the top panel for comparison to reaction
169 products (right axis).

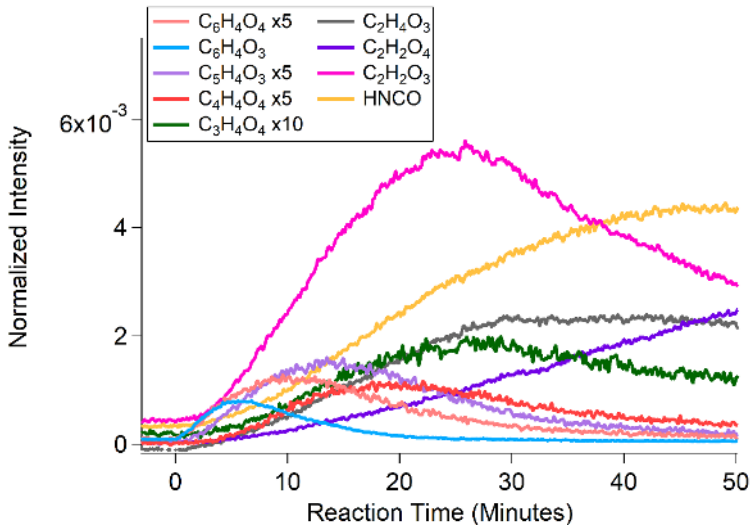

Figure S10. Formation of fragmentation products as a function of reaction time from the photo-oxidation of dinitrophenol. The signal from each molecule is normalized to the acetate reagent ion to give the normalized intensity.

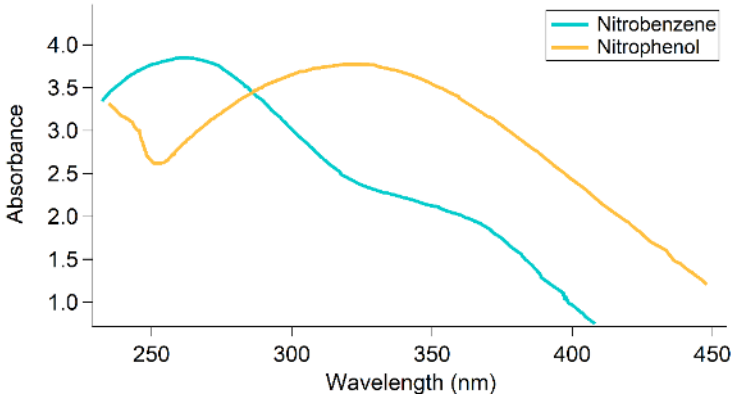

Figure S11. Comparison of the UV-visible absorbance spectrum of nitrobenzene and nitrophenol, showing the effect of an added hydroxyl group. Data obtained from the NIST chemistry WebBook *http://webbook.nist.gov/chemistry/*.

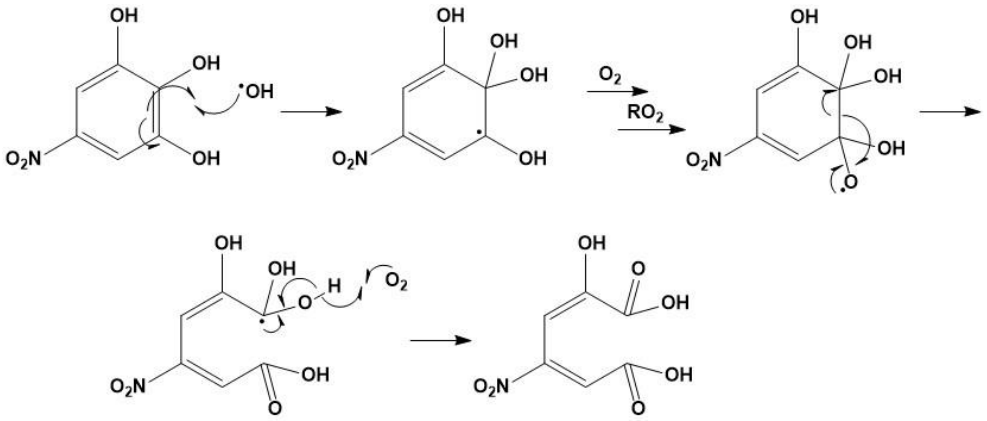

179

180 **Figure S12**. Proposed OH-initiated ring opening mechanism for a nitrocatechol oxidation product.

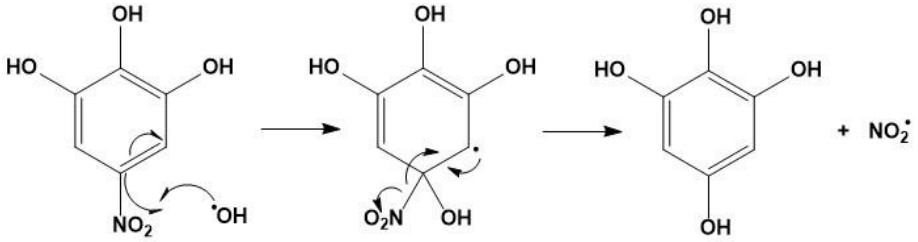

181

182 **Figure S13.** Proposed nitro-group loss mechanism by attack of OH radical at the nitro-substituted
183 carbon, shown for a nitrocatechol oxidation product.

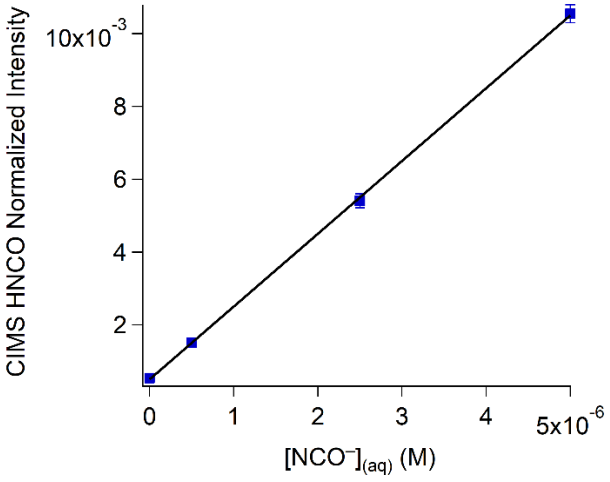

184

185 **Figure S14.** Aerosol-CIMS calibration of HNCO signal as a function of dissolved concentration
186 of isocyanate.

187

References

(1) Herrmann, H.; Schaefer, T.; Tilgner, A.; Styler, S. A.; Weller, C.; Teich, M.; Otto, T. Tropospheric Aqueous-Phase Chemistry: Kinetics, Mechanisms, and Its Coupling to a Changing Gas Phase. *Chem. Rev.* **2015**, *115* (10), 4259–4334.

(2) Zhao, R.; Mungall, E. L.; Lee, A. K. Y.; Aljawhary, D.; Abbatt, J. P. D. Aqueous-Phase Photooxidation of Levoglucosan - A Mechanistic Study Using Aerosol Time-of-Flight Chemical Ionization Mass Spectrometry (Aerosol ToF-CIMS). *Atmos. Chem. Phys.* **2014**, *14*, 9695–9705.

(3) Epstein, S. A.; Nizkorodov, S. A. A Comparison of the Chemical Sinks of Atmospheric Organics in the Gas and Aqueous Phase. *Atmos. Chem. Phys.* **2012**, *12*, 8205–8222.